Inorganic Chemistry

Article

pubs.acs.org/IC

Dinuclear Zinc(II) Complexes with Hydrogen Bond Donors as Structural and Functional Phosphatase Models

Simone Bosch,[†,‡] Peter Comba,*[,†] Lawrence R. Gahan,[‡] and Gerhard Schenk[‡]

[†]Anorganisch-Chemisches Institut, Universität Heidelberg, INF 270, D-69120, Heidelberg, Germany

[‡]School of Chemistry and Molecular Biosciences, University of Queensland, Brisbane, QLD 4072, Australia

Supporting Information

ABSTRACT: It is becoming increasingly apparent that the secondary coordination sphere can have a crucial role in determining the functional properties of biomimetic metal complexes. We have therefore designed and prepared a variety of ligands as metallo-hydrolase mimics, where hydrogen bonding in the second coordination sphere is able to influence the structure of the primary coordination sphere and the substrate binding. The assessment of a structure−function relationship is based on derivates of 2,6-bis{[bis(pyridin-2-ylmethyl)amino]methyl}-4-methylphenol (HBPMP = HL^1) and 2-{[bis(pyridin-2-ylmethyl)amino]methyl}-6-{[(2-hydroxybenzyl)(pyridin-2-ylmethyl)amino]methyl}-4-methylphenol (H_2BPBPMP = H_2L^5), well-known phenolate-based ligands for metallo-hydrolase mimics. The model systems provide similar primary coordination spheres but site-specific modifications in the secondary coordination sphere. Pivaloylamide and amine moieties were chosen to mimic the secondary coordination sphere of the phosphatase models, and the four new ligands H_3L^2, H_3L^3, HL^4, and H_4L^6 vary in the type and geometric position of the H-bond donors and acceptors, responsible for the positioning of the substrate and release of the product molecules. Five dinuclear Zn^{II} complexes were prepared and structurally characterized in the solid, and four also in solution. The investigation of the phosphatase activity of four model complexes illustrates the impact of the H-bonding network: the Michaelis−Menten constants (catalyst−substrate binding) for all complexes that support hydrogen bonding are smaller than for the reference complex, and this generally leads to higher catalytic efficiency and higher turnover numbers.

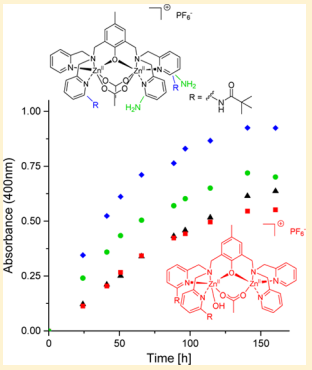

INTRODUCTION

The facile catalyzed cleavage of phosphoesters is a crucial reaction for living organisms, for example in processing RNA replication and bone metabolism, and it is of ecological importance in the detoxification of pesticides. Natural phosphatases, which accomplish this hydrolysis, commonly contain Zn^{II} ions in their active sites. Zn^{II} is frequently chosen by nature due to its high Lewis acidity, fast ligand exchange, and flexibility of the coordination geometry. Therefore, dizinc(II) complexes have been widely used as artificial models to expand our understanding of the hydrolysis mechanism in the native enzymes. Two structural forms for the binding of the substrate have been proposed, and three mechanisms of the nucleophilic attack at the phosphorus atom during the hydrolysis of phosphoesters by dinuclear metalloenzymes and their model compounds have been discussed; these structures and mechanistic proposals are depicted in Figure 1.[1−5]

Studies with model systems revealed that complexes with the two Zn^{II} ions in two different coordination geometries catalyze the hydrolysis of the highly stable P−O bond more efficiently than symmetric analogues.[4−8] These complexes also reflect structural properties of the natural enzyme more precisely. The influence of the metal ions and of the first coordination sphere has been studied in much detail previously, but the influence of the secondary coordination sphere has not been fully appreciated so far. Recent studies with ammonium, amido, or guanidine groups near the dimetal site of model complexes have demonstrated a significant impact of hydrogen bonding on the efficiency of phosphoester cleavage.[9−14] In order to study the precise role of hydrogen bonding and the magnitude of the resulting increase in reactivity, attempts have now been made to combine the two strategies, i.e., hydrogen bonding in the second coordination sphere and asymmetrization of the dinuclear coordination site, by introducing symmetric and asymmetric hydrogen bonding in model systems and investigating the emerging structural properties and phosphatase reactivities. The model systems adopted for this comparative study are the symmetric phenolate-based ligand

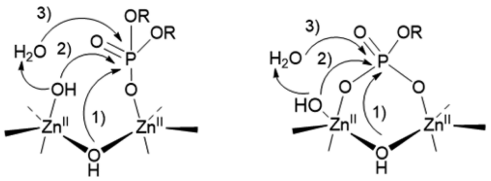

Figure 1. Proposals for the substrate binding and the three possibilities for the nucleophilic attack on the phosphorus atom during phosphoester hydrolysis by dinuclear metalloenzymes and model compounds.

Received: April 30, 2014
Published: August 14, 2014

   dx.doi.org/10.1021/ic5009945 | *Inorg. Chem.* 2014, 53, 9036−9051

HBPMP (2,6-bis{[bis(pyridin-2-ylmethyl)amino]methyl}-4-methylphenol) and its asymmetric counterpart H_2BPBPMP (2-{[bis(pyridin-2-ylmethyl)amino]methyl}-6-{[(2-hydroxybenzyl)(pyridin-2-ylmethyl)amino]methyl}-4-methylphenol), labeled HL^1 and H_2L^5 here (see Chart 1). HL^1 and H_2L^5 were derivatized with amino and pivaloylamido residues at symmetric and asymmetric positions, in order to mimic the secondary coordination sphere and analyze its influence on the symmetry of the complexes and their reactivity (Chart 1). Here we report the Zn^{II} chemistry of these ligands in terms of their reactivity as biomimetic phosphate hydrolysis catalysts.

Chart 1. Series of Ligands Discussed in This Work[a]

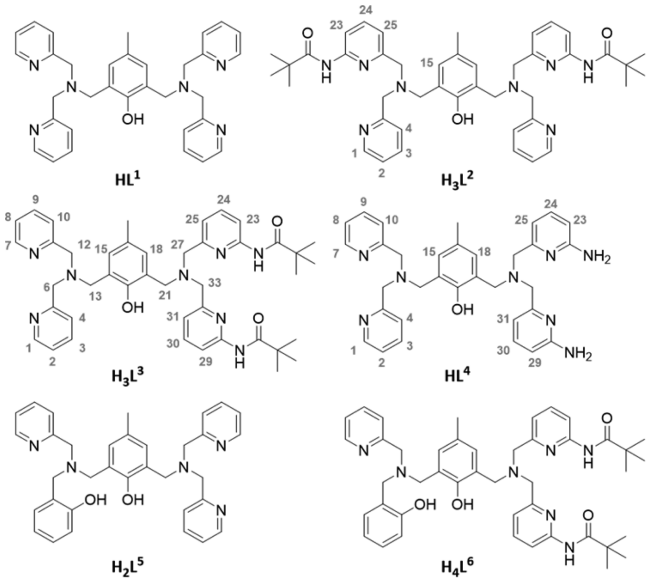

[a]Atom numbers refer to the assignments in Figures 3–6.

RESULTS AND DISCUSSION

Synthesis of the Ligands and Their Zn^{II} Complexes. The previously reported ligands HL^1 and H_3L^2 were prepared with minor modifications according to literature procedures.[13,15,16] The asymmetric ligands H_3L^3 and HL^4 were obtained by reaction of 3-(chloromethyl)-2-hydroxy-5-methylbenzaldehyde (**2**) with bis(pyridin-2-ylmethyl)amine (**1**) (Scheme 1), followed by reaction with *N,N*-bis((2-pivaloylamidopyridin-6-yl)methyl)amine (**4**), yielding ligand H_3L^3; HL^4 was generated by deprotection of the amine moieties in H_3L^3. H_4L^6 was prepared following the same procedure but using 2-(((pyridin-2-ylmethyl)amino)methyl)phenol (**1a**) as secondary amine in the first step.

The dinuclear Zn^{II} complexes of HL^1, H_3L^2, H_3L^3, HL^4, and H_4L^6 were obtained from the metal-free ligands and $Zn^{II}(OAc)_2$ in methanol. Addition of sodium hexafluoridophosphate resulted, upon standing, in X-ray quality crystals of the five complexes $[Zn_2(L^1)(OAc)_2]PF_6$, $[Zn_2(H_2L^2)(OAc)_2]PF_6$, $[Zn_2(H_2L^3)(OAc)(OH)]PF_6$, $[Zn_2(L^4)(OAc)_2]PF_6$, and $[Zn_2(H_2L^6)(OAc)(OH)]$, and the corresponding structures facilite the visualization of the H-bonding interactions, promoted by different ligands in the solid state and the analysis of the influence of the hydrogen bond donors on the coordination geometry of the two Zn^{II} centers. The structural studies in the solid were then extended to the solution state, using ^1H NMR spectroscopy, and correlated with the solution hydrolytic reactivity.

Structural Characterization of the Complexes. *Solid-State Structures.* The structures of $[Zn_2(L^1)(OAc)_2]PF_6$, $[Zn_2(H_2L^2)(OAc)_2]PF_6$, $[Zn_2(H_2L^3)(OAc)(OH)]PF_6$, $[Zn_2(L^4)(OAc)_2]PF_6$, and $[Zn_2(H_2L^6)(OAc)(OH)]$ are composed of the respective ligand anions, resulting from the deprotonation of the phenol backbone and the additional phenol moiety in H_4L^6, two Zn^{II} ions, bridging acetate anions, and a noncoordinated hexafluoridophosphate anion (except for the neutral complex $[Zn_2(H_2L^6)(OAc)(OH)]$). Selected bond lengths and valence angles of the complexes are displayed in Table 1. When $[Zn_2(H_2L^3)(OAc)(OH)]PF_6$ was reacted in acetonitrile with an excess of the unreactive phosphomonoester 4-nitrophenyl phosphate (PNPP), the substrate–catalyst adduct $[Zn_2(H_2L^3)(O_3POC_6H_4NO_2)]PF_6$ crystallized (this structure is discussed in more detail below; the structural data are included in Table 1).

While the dinuclear Zn^{II} complexes of the ligands HL^1, H_3L^2, and HL^4 show the common structure for this type of phenolate-based complex, reaction of H_3L^3 or H_4L^6 with $Zn^{II}(OAc)_2$ resulted in a different coordination geometry. In $[Zn_2(L^1)$-

Scheme 1. Synthesis of the Asymmetric Ligands H_3L^3, HL^4, and H_4L^6

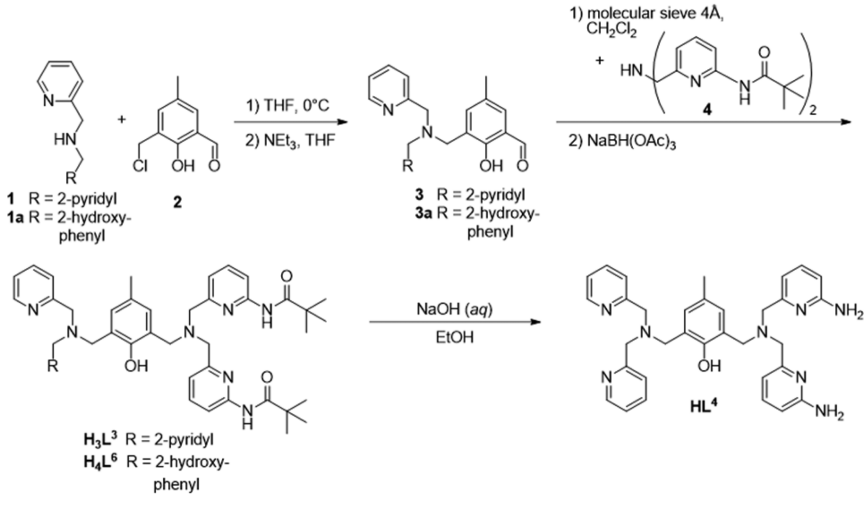

dx.doi.org/10.1021/ic5009945 | Inorg. Chem. 2014, 53, 9036–9051

Table 1. Selected Bond Lengths (Å) and Angles (deg) for $[Zn_2(L^1)(OAc)_2]PF_6$, $[Zn_2(H_2L^2)(OAc)_2]PF_6$, $[Zn_2(H_2L^3)(OAc)(OH)]PF_6$, $[Zn_2(H_2L^3)(O_3POC_6H_4NO_2)]PF_6$, $[Zn_2(L^4)(OAc)_2]PF_6$, and $[Zn_2(H_2L^6)(OAc)(OH)]$

	$[Zn_2(L^1)(OAc)_2]^+$	$[Zn_2(H_2L^2)(OAc)_2]^+$	$[Zn_2(H_2L^3)(OAc)(OH)]^+$	$[Zn_2(H_2L^3)(O_3POC_6H_4NO_2)]^+$	$[Zn_2(L^4)(OAc)_2]^+$	$[Zn_2(H_2L^6)(OAc)(OH)]$
Zn(1)···Zn(2)	3.3714(4)	3.3992(6)	3.5422(7)	3.6971(8)	3.3948(10)	3.5892(6)
Zn(1)−O(1)	2.0135(14)	2.025(3)	1.954(3)	1.987(3)	1.994(4)	1.9904(19)
Zn(1)−O(2A)	2.1825(16)	2.092(3)	2.003(3)	2.011(3)	2.112(4)	2.065(2)
Zn(1)−O(2B)	2.0088(15)	2.056(3)			2.008(4)	
Zn(1)−N(1)	2.2346(19)	2.169(3)	2.057(3)	2.074(4)	2.216(5)	2.096(2)
Zn(1)−N(2)	2.2306(19)	2.214(3)	2.233(2)	2.269(4)	2.206(5)	2.213(2)
Zn(1)−N(3)[a]	2.1443(19)	2.284(3)	2.102(3)	2.062(4)	2.132(5)	1.934(2)
Zn(2)−O(1)	2.0342(14)	2.000(3)	2.120(2)	2.140(3)	1.995(4)	2.1380(19)
Zn(2)−O(3A)[b]	2.0198(17)	2.039(3)	2.133(3)	1.941(3)	2.008(4)	2.102(2)
Zn(2)−O(3B)	2.0849(16)	2.077(3)			2.114(4)	
Zn(2)−N(4)	2.223(2)	2.155(3)	2.322(3)	2.443(4)	2.239(5)	2.295(2)
Zn(2)−N(5)	2.247(2)	2.199(3)	2.136(3)	2.133(4)	2.165(5)	2.148(2)
Zn(2)−N(6)	2.1764(19)	2.289(3)	2.336(3)	2.107(4)	2.123(5)	2.473(2)
Zn(2)−O(6)			1.945(2)			1.9571(19)
Zn(2)−O(5)				2.122(3)		
Zn(1)−O(1)−Zn(2)	112.80(7)	115.23(13)	120.75(12)	127.16(17)	116.65(18)	120.73(9)
O(1)−Zn(1)−N(1)	87.65(6)	89.95(12)	118.71(12)	136.52(16)	88.63(18)	130.04(9)
O(1)−Zn(1)−N(2)	88.88(7)	87.20(11)	91.48(11)	89.85(14)	88.12(17)	91.80(8)
O(1)−Zn(1)−N(3)[a]	163.19(7)	160.92(12)	124.82(11)	100.53(16)	161.07(18)	109.92(9)
O(1)−Zn(1)−O(2A)[b]	87.91(6)	89.64(11)	99.48(12)	98.94(13)	89.65(16)	90.21(8)
O(1)−Zn(1)−O(2B)	100.20(6)	100.55(11)			101.16(17)	
O(1)−Zn(2)−N(4)	86.73(7)	93.20(12)	88.66(10)	162.62(14)	91.46(16)	86.80(8)
O(1)−Zn(2)−N(5)	87.53(6)	88.29(12)	90.65(11)	91.55(14)	89.20(17)	91.44(9)
O(1)−Zn(2)−N(6)	163.04(7)	159.77(12)	161.27(10)	87.68(14)	162.28(16)	161.12(8)
O(1)−Zn(2)−O(3A)[b]	100.51(6)	101.25(11)	87.91(11)	93.42(13)	98.04(17)	91.27(8)
O(1)−Zn(2)−O(3B)	92.43(6)	90.00(11)			88.12(15)	
O(1)−Zn(2)−O(6)			102.84(10)			107.30(8)
O(5)−Zn(2)−O(1)				100.35(13)		

[a]In the case of $[Zn_2(H_2L^6)(OAc)(OH)]$ N(3) is O(1a). [b]In the case of $[Zn_2(H_2L^3)(OAc)(OH)]^+$, $[Zn_2(H_2L^3)(O_3POC_6H_4NO_2)]^+$, and $[Zn_2(H_2L^6)(OAc)(OH)]$ O(2A) is O(2) and O(3A) is O(3).

$(OAc)_2]PF_6$, $[Zn_2(H_2L^2)(OAc)_2]PF_6$, and $[Zn_2(L^4)(OAc)_2]$-PF_6 both Zn^{II} ions are coordinated in a six-coordinate arrangement and are bridged by the ligand backbone phenoxo group and two acetate coligands. The remaining coordination sites are occupied by the nitrogen donors of two pyridine ligands and the tertiary amines. The structure of $[Zn_2(H_2L^2)$-$(OAc)_2]PF_6$ is shown in Figure 2a.

In contrast to the other ligands, the reaction of H_3L^3 with $Zn^{II}(OAc)_2$ resulted in the asymmetric dizinc(II) complex $[Zn_2(H_2L^3)(OAc)(OH)]PF_6$ (Figure 2b). Zn(1), the Zn^{II} ion in the amide-free binding site, adopts here a pentacoordinate trigonal bipyramidal geometry (τ = 0.94; τ = 1 and τ = 0 for regular trigonal bipyramidal and square pyramidal geometries, respectively).[17] The trigonal plane is formed by the donors of two pyridines and the bridging phenoxo group, and the Zn^{II} center is out of the trigonal plane by 0.257 Å toward O(2). The axial positions are occupied by the tertiary amine and an acetate oxygen donor. The asymmetric ligand H_4L^6 forms a similar complex, $[Zn_2(H_2L^6)(OAc)(OH)]$, when treated with Zn^{II} acetate (Figure 2c). The five donors around the Zn(1) ion in $[Zn_2(H_2L^6)(OAc)(OH)]$ arrange in a coordination geometry with a τ-value of 0.58, in between a trigonal bipyramidal and a square pyramidal geometry. In both complexes $[Zn_2(H_2L^3)$-$(OAc)(OH)]PF_6$ and $[Zn_2(H_2L^6)(OAc)(OH)]$, the second Zn^{II} ion, Zn(2), is six-coordinate, similar to the Zn^{II} sites in $[Zn_2(L^1)(OAc)_2]PF_6$, $[Zn_2(H_2L^2)(OAc)_2]PF_6$, and $[Zn_2(L^4)$-$(OAc)_2]PF_6$. The two Zn^{II} ions in $[Zn_2(H_2L^3)(OAc)(OH)]$-PF_6 and $[Zn_2(H_2L^6)(OAc)(OH)]$ are doubly bridged by the phenoxo group of the supporting ligand and an acetate coligand; the coordination environment of the octahedral Zn(2) site is completed by a hydroxido group; this is unusual and confirmed by comparison with the structures of previously published Zn^{II} complexes with aqua, μ-hydroxido, and terminal hydroxido donor groups. For example, for the dizinc(II) complex of HL^1, $[Zn_2(L^1)(OH_2)_2](ClO_4)_3$, Zn−$OH_2$ distances are on the order of 2.04 Å, and the corresponding distances to bridging hydroxido ligands are reduced to 1.99 Å, as in $[Zn_2(L^1)(\mu\text{-}OH)](ClO_4)_2$.[18] Similar Zn−($\mu$-OH) distances have been found for a variety of dizinc(II) complexes: $[\{(L^7)Zn\}_2(\mu\text{-}OH)_2](ClO_4)_2]$ (1.983(3) Å; L^7 = *N*-methyl-*N*-((6-neopentylamino-2-pyridyl)methyl)-*N*-((2-pyridyl)methyl)-amine), $[\{(L^8)Zn\}_2(\mu\text{-}OH)_2](ClO_4)_2{\cdot}0.5CH_3CN]$ (2.070(3) Å; L^8 = *N*-methyl-*N*-((6-neopentylamino-2-pyridyl)methyl)-*N*-((2-pyridyl)ethyl)amine), $[Zn_2(L^9)(\mu\text{-}OH)(py)_2](ClO_4)_2]$ (1.946(3) Å; HL^9 = 2,6-bis(*N*-((2-dimethylamino)ethyl)-iminomethyl)-4-methylphenol), $[Zn_2(L^{10})(\mu\text{-}OH)(py)_3]$-$(ClO_4)_2$ (1.951(4) Å; HL^{10} = 2,6-bis(*N*-((2-pyridyl)ethyl)-iminomethyl)-4-methylphenol), $[Zn_2(L^1)(\mu\text{-}OH)](ClO_4)_2]$ (1.943(3)) Å.[18−20] Interestingly, with HL^1, there is an asymmetric acetate-bridged dizinc(III) structure with a pentacoordinate Zn^{II} site and a hexacoordinate site, similar to our structures in Figure 2b,c; however, in the published structure with HL^1, the coordination sphere of the hexacoordinate site is completed by a methanol molecule

dx.doi.org/10.1021/ic5009945 | Inorg. Chem. 2014, 53, 9036−9051

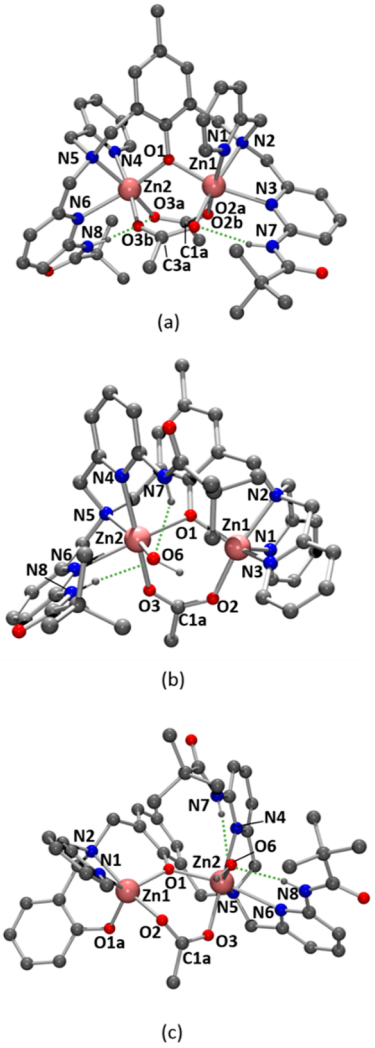

Figure 2. POV-Ray plots of (a) $[Zn_2(H_2L^2)(OAc)_2]PF_6$, (b) $[Zn_2(H_2L^3)(OAc)(OH)]PF_6$, and (c) $[Zn_2(H_2L^6)(OAc)(OH)]$, showing hydrogen bonding (green dotted lines; counterions, non-coordinated solvent molecules, and hydrogen atoms not involved in hydrogen bonding are omitted for clarity; labels are included only for atoms discussed in the text or tables; ORTEP plots with 50% probability level thermal ellipsoids of all complexes appear as Supporting Information).

with a Zn−OHMe distance of 2.0849(8) Å.[45] Therefore, the Zn−O distances in $[Zn_2(H_2L^3)(OAc)(OH)]PF_6$ (1.945(2) Å) and $[Zn_2(H_2L^6)(OAc)(OH)]$ (1.9571(19) Å) are significantly shorter than in reported complexes with terminal aqua ligands and compare with the range of complexes containing bridging hydroxides. This supports the interpretation of our data as rare examples with a terminal hydroxido group coordinated to one of the two Zn^{II} centers. Moreover, the Zn(1)···OH distances of 3.936 Å in $[Zn_2(H_2L^3)(OAc)(OH)]PF_6$ and 4.199 Å in $[Zn_2(H_2L^6)(OAc)(OH)]$ support the assignment of the OH^- group in question as a terminal hydroxido coligand.

We are not aware of any other example with a terminal hydroxido coligand in dinuclear Zn^{II} complexes with similar phenolate-based ligand scaffolds. The observation of the two hydroxido complexes is consistent with the proposition that the hydrogen bond donors, i.e., the two adjacent amide residues at the binding site of one Zn^{II} center of $[Zn_2(H_2L^3)(OAc)(OH)]PF_6$ and $[Zn_2(H_2L^6)(OAc)(OH)]$, stabilize this unusual hydroxido coligand. Moreover, the hydrogen bond donor formation within the structures of $[Zn_2(H_2L^3)(OAc)(OH)]PF_6$ and $[Zn_2(H_2L^6)(OAc)(OH)]$ is confirmed by the observed geometry of the amide hydrogen atoms with respect to the free electron pairs of the hydroxido oxygen atom. This is in agreement with the previous finding that the incorporation of two H-bond donors (neopentylamino groups) in tripodal N_4 ligands leads to the generation of the stable Zn^{II}−OH complex $[Zn(L^{11})(OH)](ClO_4)$ due to H-bonding (L^{11} = *N*,*N*-bis(6-neopentylamino-2-pyridylmethyl)-*N*-(2-pyridylmethyl)amine); $[Zn_2(H_2L^3)(OAc)(OH)]PF_6$, $[Zn_2(H_2L^6)(OAc)(OH)]$, and $[Zn(L^{11})(OH)](ClO_4)$ have a similar Zn−O distance of ∼1.94 Å.[21] Hydrogen bond formation in the mononuclear Zn^{II} complex $[Zn(L^{11})(OH)](ClO_4)$ was proposed from the short distances between the amino nitrogen and hydroxido oxygen atoms (2.741 and 2.727 Å);[21] the corresponding distances for $[Zn_2(H_2L^3)(OAc)(OH)]PF_6$ and $[Zn_2(H_2L^6)(OAc)(OH)]$ are listed in Table 2. This table also contains the corresponding distances for $[Zn_2(H_2L^2)(OAc)_2]PF_6$ and $[Zn_2(L^4)(OAc)_2]PF_6$, and those between the amine or amide nitrogen atoms and the nearby acetate oxygen atoms are in the range of 2.750 and 2.982 Å. These short distances demonstrate that the desired hydrogen bond formation is also present in these complexes. Importantly, the protons of the amine or amide moieties in question point toward the oxygen atoms of the bridging acetate groups.

In all five complexes discussed here as well as in the catalyst−substrate complex discussed below, the Zn^{II} ions are coordinated in the *anti*-configuration with respect to the phenoxide ring. The resulting $Zn^{II}\cdots Zn^{II}$ distances (see Table 1) are at the short end of the range reported for similar dinuclear Zn^{II} complexes. The variation of ligand symmetry and substituents in the range of the five ligands discussed here leads to only a relatively small variation of the $Zn^{II}\cdots Zn^{II}$ distance (3.37 to 3.59 Å, phosphate-bridged complex excluded). Importantly, the $Zn^{II}\cdots Zn^{II}$ distances are slightly elongated in the asymmetric complexes $[Zn_2(H_2L^3)(OAc)(OH)]PF_6$ and $[Zn_2(H_2L^6)(OAc)(OH)]$ to 3.54 and 3.59 Å. Consequently, the Zn^{II}−O−Zn^{II} angle is increased there to ∼120°, close to a highly symmetric trigonal angle with respect to the phenoxide bridge, and this compares with Zn^{II}−O−Zn^{II} angles in the range 112.8° to 116.1° in the more symmetric derivatives

Table 2. Selected Distances (Å) Corresponding to H-Bond Formation in $[Zn_2(H_2L^2)(OAc)_2]PF_6$, $[Zn_2(H_2L^3)(OAc)(OH)]PF_6$, $[Zn_2(L^4)(OAc)_2]PF_6$, and $[Zn_2(H_2L^6)(OAc)(OH)]$

	$[Zn_2(H_2L^2)(OAc)_2]^+$	$[Zn_2(H_2L^3)(OAc)(OH)]^+$	$[Zn_2(L^4)(OAc)_2]^+$	$[Zn_2(H_2L^6)(OAc)(OH)]$
N(7)−O(2B)	2.982(4)			
N(7)−O(3A)			2.803(9)	
N(7)−O(6)		2.810(4)		2.764(3)
N(8)−O(3A)	2.977(5)		2.750(8)	
N(8)−O(6)		2.875(4)		2.870(3)

dx.doi.org/10.1021/ic5009945 | *Inorg. Chem.* 2014, 53, 9036−9051

$[Zn_2(L^1)(OAc)_2]PF_6$, $[Zn_2(H_2L^2)(OAc)_2]PF_6$, and $[Zn_2(L^4)(OAc)_2]PF_6$. This suggests that the asymmetric ligands H_3L^3 and H_4L^6 enforce a cavity that leads to the complexation of two Zn^{II} ions in different coordination geometries: one Zn^{II} site is trigonal bipyramidal, the geometry found for both Zn^{II} ions in the active site of phospholipase C,[22] and the other Zn^{II} site in the asymmetric model system with H_3L^3 is square bipyramidal, as in the Ser/Thr phosphatase-1.[23] Interestingly and as expected, the biomimetic systems $[Zn_2(H_2L^3)(OAc)(OH)]PF_6$ and $[Zn_2(H_2L^6)(OAc)(OH)]$ demonstrate the formation of a hydrogen-bond network similar to that found in the active site of the native enzymes. The environment engendered by H_3L^3 and H_4L^6 upon complexation with Zn^{II} ions mimics the structural characteristics of the backbone built by the nucleic acids within the active site of phosphatases more accurately than other model systems published to date.

Infrared Spectroscopy. Solid-state FT-IR measurements of the metal-free ligands and the complexes were studied and compared in order to investigate the strength of hydrogen bonds (see Supporting Information for the IR spectra).[24] The very similar IR spectra of H_3L^2, H_3L^3, and H_4L^6 show the N−H vibrational band at around 3440 cm^{-1}. Due to the weakening of the N−H bond emerging from hydrogen bond formation, this N−H vibrational band is shifted to 3295 cm^{-1} in the spectrum of $[Zn_2(H_2L^2)(OAc)_2]PF_6$. In the spectra of $[Zn_2(H_2L^3)(OAc)(OH)]PF_6$ and $[Zn_2(H_2L^6)(OAc)(OH)]$ there are only very broad N−H vibrational bands, and this suggests that the hydrogen bonds are even stronger in these complexes.[24−26]

Mass Spectrometry. In order to investigate the complex structure of the dizinc(II) complexes in solution, mass spectrometric data were obtained in acetonitrile (see Supporting Information). All highest mass peaks show the distinctive isotopic pattern of dinuclear Zn^{II} complexes; the *m*/*z* separation of 0.5 between the peaks within the isotopic pattern suggests the presence of doubly charged species. In the case of $[Zn_2(L^1)(OAc)_2]PF_6$, the highest mass peak was found at *m*/*z* 360.0704 (calcd 360.0689), corresponding to $[Zn_2(L^1)(OAc)]^{2+}$. The corresponding singly charged species $[Zn_2(L^1)(OAc)]^+$ was found at *m*/*z* 779.1507 (calcd 779.1517). The highest mass peak for $[Zn_2(H_2L^2)(OAc)_2]PF_6$ at *m*/*z* 429.1283 (calcd 429.1268) was likewise assigned to $[Zn_2(H_2L^2)]^{2+}$. For $[Zn_2(H_2L^3)(OAc)(OH)]PF_6$ the highest mass peaks at *m*/*z* 429.1298 (calcd 429.1268) and *m*/*z* 917.2757 (calcd 917.2674) were assigned to $[Zn_2(H_2L^3)]^{2+}$ and $[Zn_2(H_2L^3)(OAc)]^+$. In the case of $[Zn_2(L^4)(OAc)_2]PF_6$, a $[Zn_2(L^4)]^{2+}$ species was detected with *m*/*z* 344.0730 (calcd 344.0701). The highest mass peak in the spectra of $[Zn_2(H_2L^6)(OAc)(OH)]$ was found at 435.6226 and assigned to $[Zn_2(H_2L^6)]^{2+}$.

NMR Studies. In order to study the symmetry of the complexes in solution ^1H and ^{13}C NMR spectra were measured in deuterated acetonitrile. The equivalence of the two binding sites of $[Zn_2(H_2L^2)(OAc)_2]PF_6$ on the NMR time scale was confirmed with the 16 aromatic protons resulting in eight resonances in the aromatic region of the ^1H NMR spectrum, with each of the multiplet resonances integrating for two protons. Comparison with the ^1H NMR spectrum of the metal-free ligand H_3L^2 shows a downfield shift of protons of the amidated pyridine residues and an upfield shift of protons of the unsubstituted pyridine groups upon binding to Zn^{II} (Figure 3). As expected, complex $[Zn_2(L^1)(OAc)_2]PF_6$ shows an analogous behavior, leading to a ^1H NMR spectrum corresponding to a pair of two identical picolyl groups within the complex. Moreover, only one resonance for the *tert*-butyl group of H_2L^2 as well as for the acetate coligands was visible in the ^1H NMR spectrum of $[Zn_2(H_2L^2)(OAc)_2]^+$ (see Supporting Information). ^1H NMR measurements were also conducted in mixtures of CD_3CN/D_2O, which resulted in similar resonances, leading to identical interpretations, but with lower resolution of the spectra. Importantly, the stepwise addition of sodium deuteroxide (up to a pH value of 10.5 for the deuterium oxide phase) did not show a significant shift of the resonances (see Supporting Information).

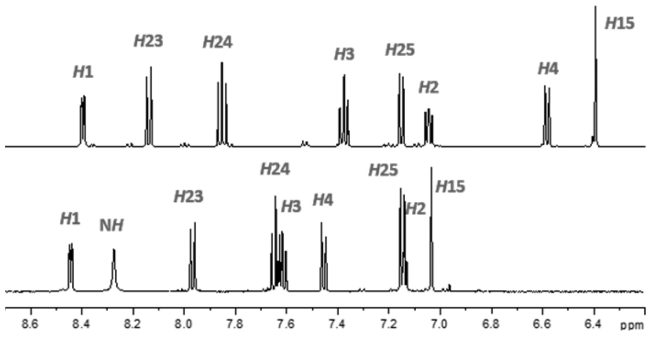

Figure 3. Aromatic region of the ^1H NMR spectra of H_3L^2 (bottom) and $[Zn_2(H_2L^2)(OAc)_2]^+$ (top) in CD_3CN.

The asymmetry of $[Zn_2(H_2L^3)(OAc)(OH)]^+$ in solution (similar to the observations in the solid, see above) emerges from its ^1H NMR spectrum, where the aromatic region exhibits 16 resonances (Figure 4, top). In this complex, every hydrogen atom has a different electronic environment, leading to the difference in the spectrum, when compared to the metal-free ligand (Figure 4, bottom). The resonances from the protons proximal to the Zn^{II} centers show a downfield shift, while protons that are distant from the metal centers, especially those pointing to the opposite side of the phenolate backbone, show an upfield shift. Similarly, the proton signals of each methylene group are separated, which gives rise to a set of 12 doublets in the region between 3.3 and 4.5 ppm (Figure 5, top). This implies that the electronic environment of protons bound to the same methylene carbon are not identical, in contrast to the spectrum of the free ligand (Figure 5, bottom), and this again is consistent with the observed X-ray structure (see above). The coupling to the other hydrogen atom of the same carbon center leads to the appearance of doublets. As a result of the asymmetry within this structure, the two *tert*-butyl groups in $[Zn_2(H_2L^3)(OAc)(OH)]^+$ give rise to two resonances in the ^1H NMR spectrum. Unfortunately, the poor solubility of $[Zn_2(H_2L^6)(OAc)(OH)]$ made it impossible to conduct a comparable set of ^1H NMR measurements for this complex.

Although the crystal structure of $[Zn_2(L^4)(OAc)_2]PF_6$ suggests that, in the solid state, the complex is symmetric, the ^1H NMR spectrum exhibits 16 resonances in the aromatic region (Figure 6, top). In contrast to $[Zn_2(H_2L^2)(OAc)_2]^+$, the two bridging acetate coligands in $[Zn_2(L^4)(OAc)_2]^+$ produce two resonances in the ^1H NMR spectrum. Therefore, the substitution of two pyridine groups in one of the binding sites of HL^1 creates two different coordination environments in HL^4, which induce the formation of an asymmetric dinuclear Zn^{II} complex in solution, in contrast to the symmetric structure observed in the solid state by X-ray crystallography (see above). This suggests that the asymmetry of the amide-based complex $[Zn_2(H_2L^3)(OAc)(OH)]PF_6$ not only is the result of the two different coordination geometries of the two Zn^{II} centers but is

dx.doi.org/10.1021/ic5009945 | *Inorg. Chem.* 2014, 53, 9036−9051

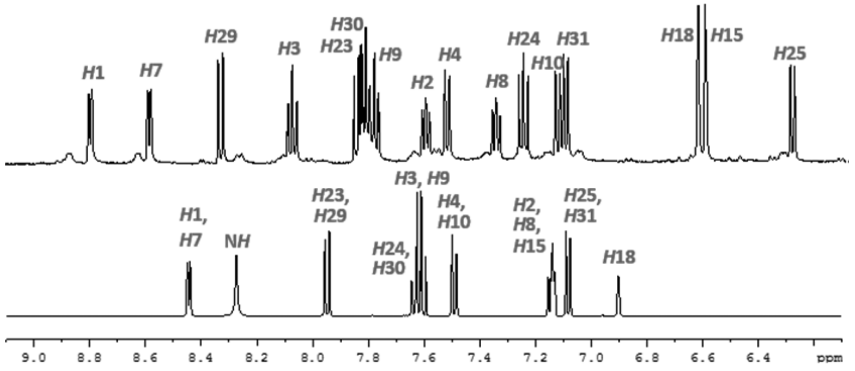

Figure 4. Aromatic region of the ^{1}H NMR spectra of H_3L^3 (bottom) and $[Zn_2(H_2L^3)(OAc)(OH)]^+$ (top) in CD_3CN.

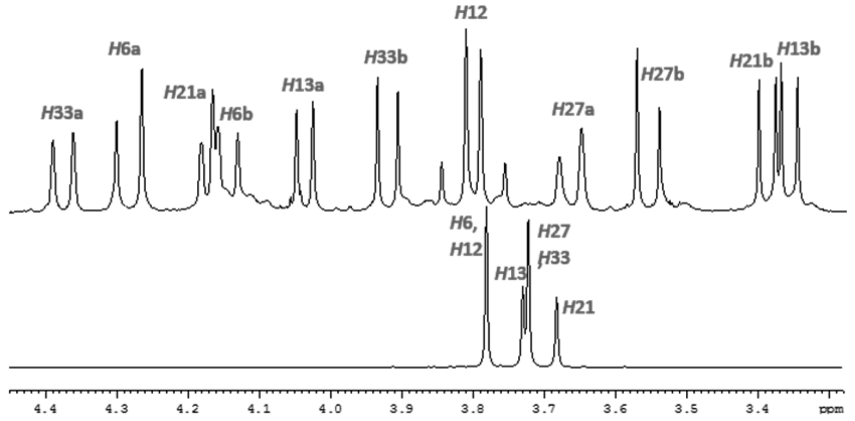

Figure 5. Methylene proton signals in the ^{1}H NMR spectra of H_3L^3 (bottom) and $[Zn_2(H_2L^3)(OAc)(OH)]^+$ (top) in CD_3CN.

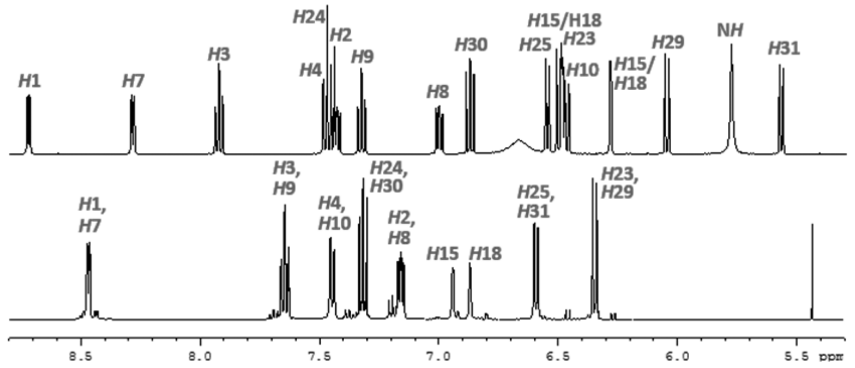

Figure 6. Aromatic region of the ^{1}H NMR spectra of HL^4 (bottom) and $[Zn_2(L^4)(OAc)_2]^+$ (top) in CD_3CN.

also due to the H-bond donating groups in proximity to one of the coordination sites.

Electronic Properties. Electronic spectrum of the complexes $[Zn_2(L^1)(OAc)_2]PF_6$, $[Zn_2(H_2L^2)(OAc)_2]PF_6$, $[Zn_2(H_2L^3)(OAc)(OH)]PF_6$, and $[Zn_2(L^4)(OAc)_2]PF_6$ were recorded in acetonitrile (Figure 7). All four dinuclear Zn^{II} complexes show two bands in the regions of 230−260 and 280−320 nm, respectively, attributed to $p\pi \rightarrow p\pi^*$ ligand internal transitions. The substitution with a pivaloyl amido group in position six of two pyridine residues in $[Zn_2(H_2L^2)(OAc)_2]PF_6$ and $[Zn_2(H_2L^3)(OAc)(OH)]PF_6$ leads to a hypsochromic effect in the UV−vis spectroscopic measurements, compared with the spectrum of the unsubstituted compound $[Zn_2(L^1)(OAc)_2]PF_6$. The substitution by amino moieties instead, as in $[Zn_2(L^4)(OAc)_2]PF_6$, has a similar but less pronounced effect.

In order to study the behavior of the complexes $[Zn_2(H_2L^2)(OAc)_2]^+$, $[Zn_2(H_2L^3)(OAc)(OH)]^+$, and $[Zn_2(L^4)(OAc)_2]^+$ under basic conditions, UV−vis spectroscopic measurements were also conducted in acetonitrile/aqueous buffer mixtures (1:1). The aqueous buffer consisted of 2-(*N*-morpholino)-ethanesulfonic acid (MES), 4-(2-hydroxyethyl)piperazine-1-ethanesulfonic acid (HEPES), 2-(cyclohexylamino)-ethanesulfonic acid (CHES), 3-(cyclohexylamino)-1-propanesulfonic acid (CAPS), and lithium perchlorate for ionic strength control and was adjusted to a specific pH value by addition of aqueous sodium hydroxide solution (see also Kinetic Studies, below). The same buffer solutions were also used for the hydrolytic activity assays discussed in the next section.

With increasing basicity, the band in the absorbance spectrum of $[Zn_2(H_2L^2)(OAc)_2]^+$ at 287 nm experiences a shift to 294 nm. Also, the band at 233 nm decreases in

dx.doi.org/10.1021/ic5009945 | *Inorg. Chem.* 2014, 53, 9036−9051

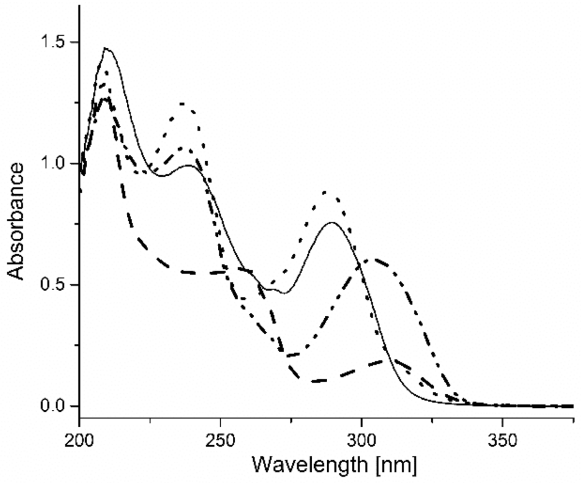

Figure 7. UV−vis absorption spectra in CH_3CN of $[Zn_2(L^1)(OAc)_2]^+$ (dashed line), $[Zn_2(H_2L^2)(OAc)_2]^+$ (dotted line), $[Zn_2(H_2L^3)(OAc)(OH)]^+$ (solid line), and $[Zn_2(L^4)(OAc)_2]^+$ (dash dotted line).

Table 3. UV−Vis Spectral Properties of $[Zn_2(L^1)(OAc)_2]^+$, $[Zn_2(H_2L^2)(OAc)_2]^+$, $[Zn_2(H_2L^3)(OAc)(OH)]^+$, and $[Zn_2(L^4)(OAc)_2]^+$ in CH_3CN

complex	UV−vis [nm]	ε [L mol^{-1} cm^{-1}]	transition
$[Zn_2(L^1)(OAc)_2]^+$	260	113 168	pπ → pπ^*
	311	37 161	pπ → pπ^*
$[Zn_2(H_2L^2)(OAc)_2]^+$	238	249 438	pπ → pπ^*
	289	177 075	pπ → pπ^*
$[Zn_2(H_2L^3)(OAc)(OH)]^+$	239	198 843	pπ → pπ^*
	290	151 351	pπ → pπ^*
$[Zn_2(L^4)(OAc)_2]^+$	237	213 347	pπ → pπ^*
	305	120 667	pπ → pπ^*

intensity, while new bands at 259 and 326 nm arise (Figure 8a). Figure 8b shows the change of absorbance at different wavelengths as a function of rising pH value. The overlay of the spectra at different pH values indicates the presence of three isosbestic points at 246, 270, and 297 nm. Fitting of the pH-dependent spectroscopic data to eq 1 leads to the pK_a value of $[Zn_2(H_2L^2)(OAc)_2]^+$: pK_a = 8.14 ± 0.25 (ε_1: extinction coefficient of protonated complex cation, ε_2: extinction coefficient of deprotonated complex cation, c_0: initial complex concentration, d: path length).

$$\text{Abs} = (\varepsilon_1 - \varepsilon_2)\frac{c_0 d}{10^{\text{pH}-\text{p}K\text{a}} + 1} + \varepsilon_2 c_0 d \qquad (1)$$

pH-dependent UV−vis spectroscopic measurements of $[Zn_2(H_2L^3)(OAc)(OH)]^+$ show similar effects (Figure 8c,d), and from fitting of these data to eq 1, the pK_a value of $[Zn_2(H_2L^3)(OAc)(OH)]^+$ was obtained: pK_a = 7.27 ± 0.65. Unfortunately, the variation of the pH value from 5 to 11 did not result in any change of the UV−vis spectra of $[Zn_2(L^1)(OAc)_2]PF_6$ and $[Zn_2(L^4)(OAc)_2]PF_6$.

The spectrophotometrically determined pK_a values of $[Zn_2(H_2L^2)(OAc)_2]^+$ and $[Zn_2(H_2L^3)(OAc)(OH)]^+$ can be compared to corresponding data obtained from the analysis of the kinetic data of the phosphoester hydrolysis, and this supports the mechanistic interpretation (see below). Importantly, the data described here also support the solution structural analysis; that is, the observation of isosbestic points in the pH range of 5 to 11 indicates that dizinc(II) complexes are stable (and the only species of relevance) in these solutions, and this emerges also from the NMR studies, specifically in mixed CD_3CN/D_2O solutions at varying pH values (see above and Supporting Information).

Kinetic Studies. *pH and Concentration Dependence.* The influence of hydrogen bonding on the phosphoester hydrolysis reactivity was probed with a spectrophotometric assay using BDNPP (bis(2,4-dinitrophenyl)phosphate) as substrate. Cleavage of the phosphorus−oxygen bond was followed at 25 °C by monitoring the generated product, 4-nitrophenolate, by its strong absorption at 400 nm (ε = 12 100 M^{-1} cm^{-1}). All measurements were carried out in an 1:1 acetonitrile/buffer mixture. The aqueous buffer consisted of MES, HEPES, CHES, CAPS, and lithium perchlorate for ionic strength control. By varying the pH of the multicomponent buffer, the pH dependence of the activity was studied in the pH range of 5 to 11 (Figure 9a). The pH values refer to the aqueous component, and it should be noted that the pH of an aqueous solution of the buffer is the same within error as in a 1:1 mixture of buffer and acetonitrile.[8,27] The resulting data were fitted to eq 2, which is based on a model for a diprotic system with two active species.[28]

$$v_0 = \frac{v_{\max}\left(1 + \frac{\gamma K_{a_2}}{[H^+]}\right)}{\left(1 + \frac{[H^+]}{K_{a_1}} + \frac{K_{a_2}}{[H^+]}\right)} \qquad (2)$$

Here, v_0 is the initial reaction rate and v_{max} is the maximum reaction rate that is reached under given conditions. The factor γ is related to the relative activity of the two active species in equilibrium (E^nS and $E^{n-1}S$); a value of γ less than unity corresponds to a more active E^nS adduct, and a value higher than 1 considers the deprotonated adduct $E^{n-1}S$ as more active.[28,29] The K_a values obtained are the protonation equilibrium constants between the two relevant active species. The resulting pK_a and γ values are listed in Table 4. The rate vs pH profiles for three of the dizinc(II) complexes show a nearly sigmoidal shape, whereas the corresponding profile for $[Zn_2(H_2L^3)(OAc)(OH)]^+$ appears to be bell-shaped. This bell-shaped profile indicates that the catalyst−substrate complex (E^nS) is most active in its mixed protonation state, whereas both protonation and deprotonation lead to a decrease of activity. Based on a fit adopting the equation for a monoprotic system, the assumed two active species in the case of $[Zn_2(L^1)(OAc)_2]^+$ and $[Zn_2(HL^4)(OAc)_2]^+$ have the same activity. In contrast, the deprotonated active species of $[Zn_2(H_2L^2)(OAc)_2]^+$ appears to play an important role in the catalytic cycle, as the rate vs pH profile rises steadily as the pH increases, leading to a γ value of 4.19. Comparison of the profiles leads to the conclusion that the presence of two amine groups near one Zn^{II} center in $[Zn_2(L^4)(OAc)_2]^+$ lowers the kinetically relevant pK_a value by 1.3 pK_a units, in agreement with previously published results.[30] The influence of two amide groups at one Zn^{II} center in $[Zn_2(H_2L^3)(OAc)(OH)]^+$ is comparatively small; in contrast the symmetric incorporation of two amide moieties in $[Zn_2(H_2L^2)(OAc)_2]^+$ causes a significant effect, both in the profile shape (highest reactivity at high pH; Figure 7a) and in the pK_a values.

The measurements of the dependence of the BDNPP hydrolysis rate on the complex concentration were determined at three pH values (i.e., pH = 7.0, 9.5, and 11) to assess the

dx.doi.org/10.1021/ic5009945 | Inorg. Chem. 2014, 53, 9036−9051

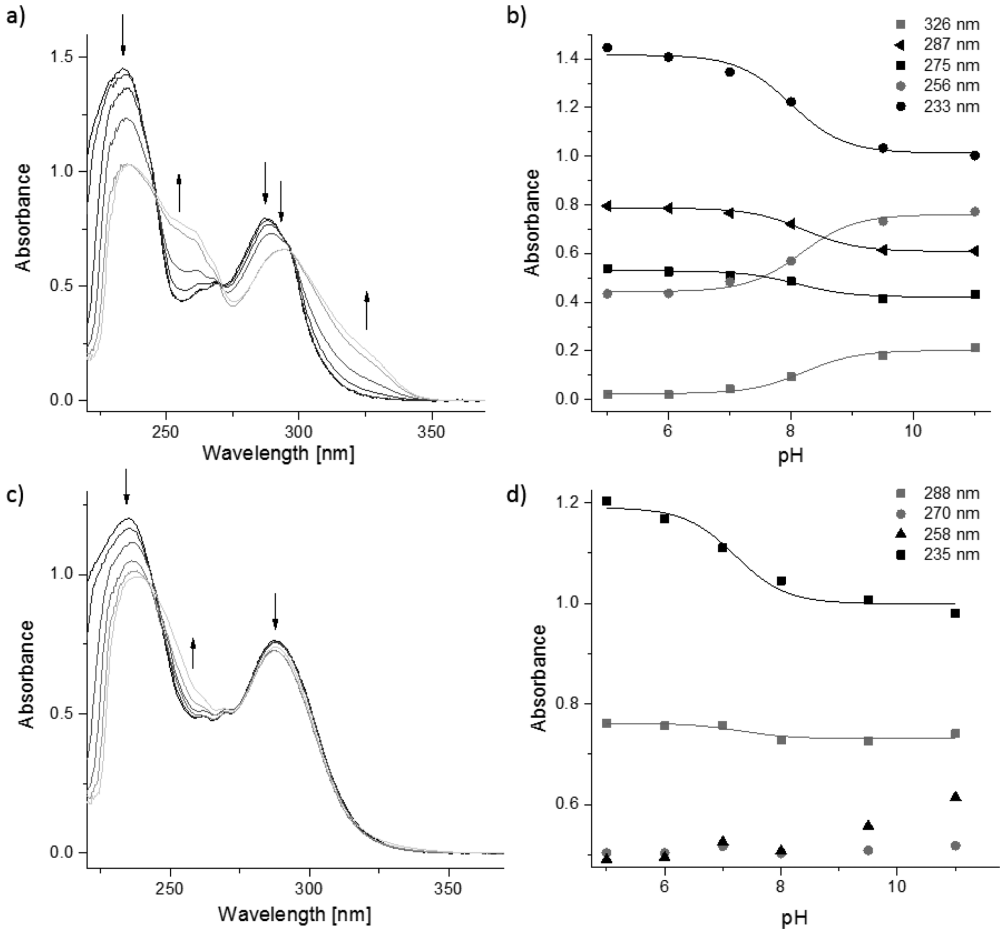

Figure 8. UV–vis spectroscopic titration spectra (5 μM in acetonitrile/buffer between pH 5 and 11) and absorbance vs pH plots for $[Zn_2(H_2L^2)(OAc)_2]^+$ (a, b) and $[Zn_2(H_2L^3)(OAc)(OH)]^+$ (c, d).

catalytic behavior of different protonation states (Figure 9b,c,d). $[Zn_2(L^4)(OAc)_2]^+$ was not tested at pH = 11, as no difference in the hydrolysis rate, compared to pH = 9.5, was detected during the previous pH dependence experiments. The results show that for each complex the hydrolysis rates are linearly dependent on the complex concentration. The dependence of the rate of hydrolysis on the BDNPP concentration shows Michaelis–Menten saturation behavior for all complexes. Due to the poor solubility of BDNPP in acetonitrile, assays with a starting concentration of the substrate higher than 11.5 mM could not be investigated. The experimental data were fitted to eq 3, and the parameter values K_m, v_{max}, and k_{cat} are listed in Table 4.

$$v_0 = \frac{v_{max}[BDNPP]_0}{K_m + [BDNPP]_0} \quad (3)$$

$$k_{cat} = \frac{v_{max}}{[complex]_0} \quad (4)$$

While at pH = 7 $[Zn_2(L^1)(OAc)_2]^+$, without hydrogen bond donors, exhibits the highest rate of hydrolysis, $[Zn_2(L^4)(OAc)_2]^+$ is the most efficient catalyst due to its smaller K_m value. Moreover, the Michaelis–Menten constants K_m are lower for all complexes providing a hydrogen bond network, compared to $[Zn_2(L^1)(OAc)_2]^+$, both at pH = 7 and pH = 9.5. The net interpretation of this observation is that complexes that facilitate hydrogen bonding exhibit higher affinities toward the phosphodiester substrate and therefore reveal higher catalytic efficiencies than $[Zn_2(L^1)(OAc)_2]^+$ (except for $[Zn_2(H_2L^2)(OAc)_2]^+$ at pH = 7).

Furthermore, the measurements at pH = 11 resulted in significantly higher k_{cat} values for the complexes that support hydrogen bond formation, compared to the reference complex $[Zn_2(L^1)(OAc)_2]^+$. The Michaelis–Menten constants obtained under these more basic conditions are comparable for all three complexes. Therefore, the complexes $[Zn_2(H_2L^3)(OAc)(OH)]^+$ and $[Zn_2(H_2L^2)(OAc)_2]^+$ have two and five times higher catalytic efficiencies than $[Zn_2(L^1)(OAc)_2]^+$.

Product Inhibition at the Active Site. Similar to the phosphate inhibition of phosphatases,[31,32] the formation of an adduct with a bridging phosphomonoester between the two Zn^{II} sites is known to lead to inhibition of phosphoester hydrolysis in model complexes.[33] Therefore, the influence of addition of DNPP to the reaction mixtures was explored (see Supporting Information). The presence of DNPP (1 mM) in the kinetic assays was shown to decrease the hydrolytic rate, independently of whether the phosphomonoester was added before or simultaneously with the substrate BDNPP (see Supporting Information). The inhibited hydrolysis rates obtained in the presence of catalyst are, within the relatively large errors of these measurements, indistinguishable from the autohydrolysis rates under the same conditions (autohydrolysis experiments contain only phosphomono- and phosphodiester). These results demonstrate not only product inhibition but also

dx.doi.org/10.1021/ic5009945 | Inorg. Chem. 2014, 53, 9036–9051

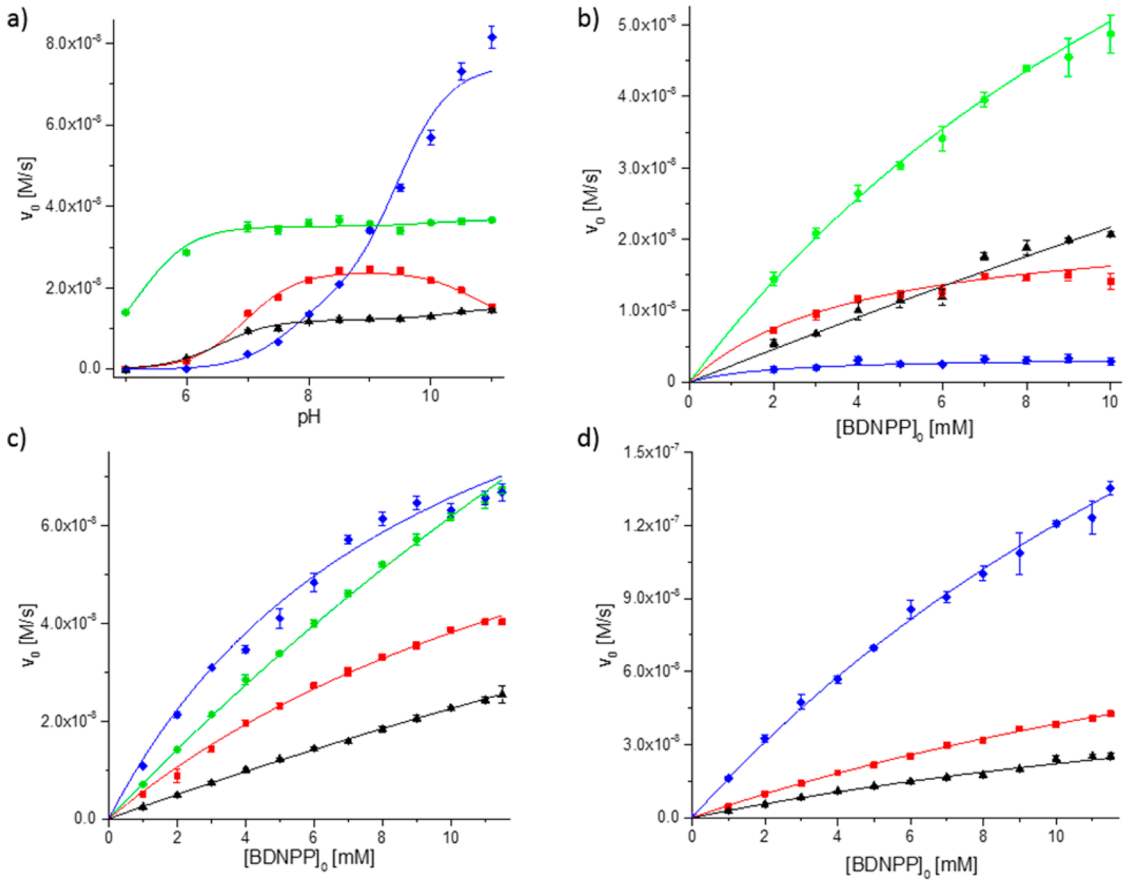

Figure 9. pH dependence of BDNPP hydrolysis activity for $[Zn_2(L^1)(OAc)_2]^+$ (black triangles), $[Zn_2(H_2L^2)(OAc)_2]^+$ (blue diamonds), $[Zn_2(H_2L^3)(OAc)(OH)]^+$ (red squares), and $[Zn_2(L^4)(OAc)_2]^+$ (green circles) (a) and substrate concentration dependence at pH = 7 (b), pH = 9.5 (c), and pH = 11 (d).

Table 4. Kinetic Data (k_{cat} in $[10^{-3}\ s^{-1}]$, K_m in [mM], and k_{cat}/K_m in $[10^{-3}\ s^{-1}mM^{-1}]$) of BDNPP Hydrolysis for $[Zn_2(L^1)(OAc)_2]^+$, $[Zn_2(H_2L^2)(OAc)_2]^+$, $[Zn_2(H_2L^3)(OAc)(OH)]^+$, and $[Zn_2(L^4)(OAc)_2]^+$

	pH	$[Zn_2(L^1)(OAc)_2]^+$	$[Zn_2(H_2L^2)(OAc)_2]^+$	$[Zn_2(H_2L^3)(OAc)(OH)]^+$	$[Zn_2(L^4)(OAc)_2]^+$
pK_{a1}		6.5	7.7	7.0	5.2
pK_{a2}		10.3	9.5	10.7	10.0
γ		1.26 ± 0.08	4.19 ± 0.67	0.45 ± 0.14	1.05 ± 0.03
k_{cat}	7	7.18 ± 4.39	0.09 ± 0.01	0.57 ± 0.04	3.49 ± 0.25
K_m	7	123 ± 79	2 ± 1	4 ± 1	18 ± 2
k_{cat}/K_m	7	0.06	0.04	0.14	0.20
k_{cat}	9.5	5.08 ± 0.85	3.20 ± 0.21	2.70 ± 0.21	9.58 ± 0.70
K_m	9.5	80 ± 14	9 ± 1	18 ± 2	52 ± 4
k_{cat}/K_m	9.5	0.06	0.34	0.15	0.18
k_{cat}	11	2.07 ± 0.29	10.83 ± 0.62	3.68 ± 0.25	
K_m	11	27 ± 5	26 ± 2	28 ± 2	
k_{cat}/K_m	11	0.08	0.42	0.13	
TON (after 8 d)	9.5	109 ± 5	158 ± 8	101 ± 4	121 ± 6

that the hydrolysis product DNPP is more strongly bound to the complex than the phosphodiester substrate BDNPP.

Turnover Numbers. Studies of the turnover number (TON) were conducted at pH = 9.5 and 25 °C with [complex] = 15 nM and [BDNPP] = 5.25 μM. Samples were taken at various intervals during the experiment and diluted with solvent, and their UV−vis spectra were recorded to determine the amount of phosphoester hydrolysis. The increase in the absorbance at 400 nm, assigned to the hydrolysis product 2,4-dinitrophenolate, was monitored over time, and TON values after 8 days were calculated using the Beer−Lambert law. The resulting data are given in Figure 10 and Table 4.

Complexes generated from ligands that engender asymmetry exhibit a lower TON than the symmetric complex $[Zn_2(H_2L^2)(OAc)_2]^+$. This implies that the presence of an amide moiety on each coordination site has a beneficial impact on the hydrolytic activity. The comparison of the time-dependent traces for the two asymmetric catalysts $[Zn_2(H_2L^3)(OAc)(OH)]^+$ and $[Zn_2(L^4)(OAc)_2]^+$ indicates that there is also a decrease of the TON as a result of the bulky nature of the pivaloyl group in the former complex. Therefore, the hydrolysis

dx.doi.org/10.1021/ic5009945 | Inorg. Chem. 2014, 53, 9036−9051

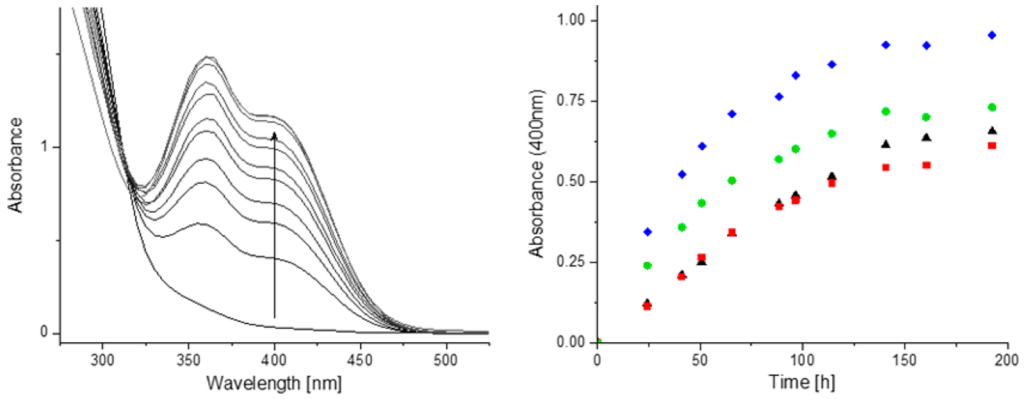

Figure 10. UV−vis spectra of the BDNPP hydrolysis assay with $[Zn_2(H_2L^2)(OAc)_2]^+$, taken at different time points after substrate addition (left) and time dependence of the absorbance band of 2,4-nitrophenolate (400 nm) with $[Zn_2(L^1)(OAc)_2]^+$ (black triangles), $[Zn_2(H_2L^2)(OAc)_2]^+$ (blue diamonds), $[Zn_2(H_2L^3)(OAc)(OH)]^+$ (red squares), and $[Zn_2(L^4)(OAc)_2]^+$ (green circles) (right).

rate of $[Zn_2(L^4)(OAc)_2]^+$ is, in the first 70 h, significantly higher. Furthermore, the data obtained with $[Zn_2(H_2L^3)(OAc)(OH)]^+$ are similar compared to those of the reference system $[Zn_2(L^1)(OAc)_2]^+$ during the first 150 h after BDNPP addition, but the difference in the traces after 150 h reveals earlier inhibition in the presence of two amide moieties at one of the two zinc(II) centers. It is proposed that an increased affinity for the hydrolysis product DNPP is the reason for this, resulting in the inhibition of the complex at an earlier point in time. The experiments demonstrate that the phosphoester hydrolysis rate of dizinc(II) complexes is influenced by (i) the availability of the catalytic center and (ii) the possibility to interact with amine or amido hydrogen bond donors, whereas the opportunity for the formation of hydrogen bonds on both metal centers appears to have a beneficial effect. Studies with a variety of complexes of bis[bis(2-substituted-pyridinyl-6-methyl)]amine type ligands have illustrated the impact of (i) enhanced H-bonding effects in the second coordination sphere, (ii) the steric hindrance in the active site and beyond, and (iii) the polarity of the substituents on the intramolecular hydrolysis of the substrate, for example, the RNA model HpNPP (2-hydroxypropyl *p*-nitrophenyl phosphate).[14] Moreover, an impaired BDNPP affinity was found for the dizinc(II) complex of a bulky phenolate-based ligand (2-(((2-methoxyethyl)(pyridine-2-ylmethyl)amino)methyl)-4-methyl-6-(((pyridin-2-ylmethyl)(4-vinylbenzyl)amino)methyl)phenol) compared to its unconcealed counterpart (2-(((2-methoxyethyl)(pyridine-2-ylmethyl)amino)methyl)-4-methyl-6-(((pyridin-2-ylmethyl)amino)methyl)phenol), which was proposed to be a steric effect attributed to the bulky vinylbenzyl group.[8] Therefore, the exact origin of the acceleration of the BDNPP hydrolysis with the dizinc(II) complexes studied in this work may be attributed in part to the enhanced H-bonding effects, but the effects of other parameters in combination with H-bonding need also to be considered.

Crystal Structure of an Asymmetric Dizinc(II) Complex with the Phosphomonoester PNPP. In order to explore the nature of product inhibition, the asymmetric complex $[Zn_2(H_2L^3)(OAc)(OH)]^+$ was treated with an excess of the phosphomonoester 4-nitrophenyl phosphate in acetonitrile. PNPP was chosen as phosphomonoester substrate mimic due to its higher stability toward autohydrolysis compared to DNPP. After the solvent was removed and the remaining oil dissolved in methanol, colorless crystals suitable for X-ray crystallography were obtained by slow evaporation. The structure reveals that the inhibited complex contains one μ-PNPP molecule, which forms a bridge between the two Zn^{II} centers of the dizinc(II) complex (Figure 11; selected structural

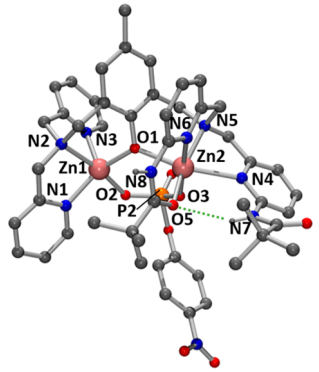

Figure 11. POV-Ray plot of $[Zn_2(H_2L^3)(O_3POC_6H_4NO_2)]PF_6$ (counterions, noncoordinated solvent molecules, and H atoms not involved in H-bonding are omitted for clarity; labels not mentioned in text or Table 1 are omitted; an ORTEP plot with 50% probability level of thermal ellipsoids appears as Supporting Information).

parameters are included in Table 1), in contrast to a previously published complex, $[Zn_4(L^{12})_2(O_3POC_6H_4NO_2)(H_2O)_2](PF_6)_2$ (L^{12} = 2,6-bis(((2-methoxyethyl)(pyridin-2-ylmethyl)amino)methyl)-4-methylphenol), in which the PNPP molecule forms not only an intramolecular bridge between the two Zn^{II} ions but also an intermolecular bridge between two Zn^{II} centers of adjacent dizinc(II) complexes.[34] In $[Zn_2(H_2L^3)(O_3POC_6H_4NO_2)]PF_6$, both Zn^{II} ions are bound to the bridging phenoxo residue, to the nitrogen atoms of two pyridine ligands, to a tertiary amine, and additionally to an oxygen atom of the bridging PNPP molecule.

Comparison with the structure of the corresponding acetate-bridged complex $[Zn_2(H_2L^3)(OAc)(OH)]PF_6$ (Figure 2b), used as the starting material for the synthesis of $[Zn_2(H_2L^3)(O_3POC_6H_4NO_2)]PF_6$, illustrates important similarities: the Zn^{II} ions in both structures are on different sides of the phenoxo plane and exhibit different coordination geometries. In the catalyst-inhibitor adduct $[Zn_2(H_2L^3)(O_3POC_6H_4NO_2)]PF_6$, Zn(1) is also coordinated in a trigonal bipyramidal geometry (τ-value of 0.88), while Zn(2) is at the center of a six-coordinate site. In contrast to the catalyst complex, the remaining coordination site of Zn(2) is no longer completed

dx.doi.org/10.1021/ic5009945 | *Inorg. Chem.* 2014, 53, 9036−9051

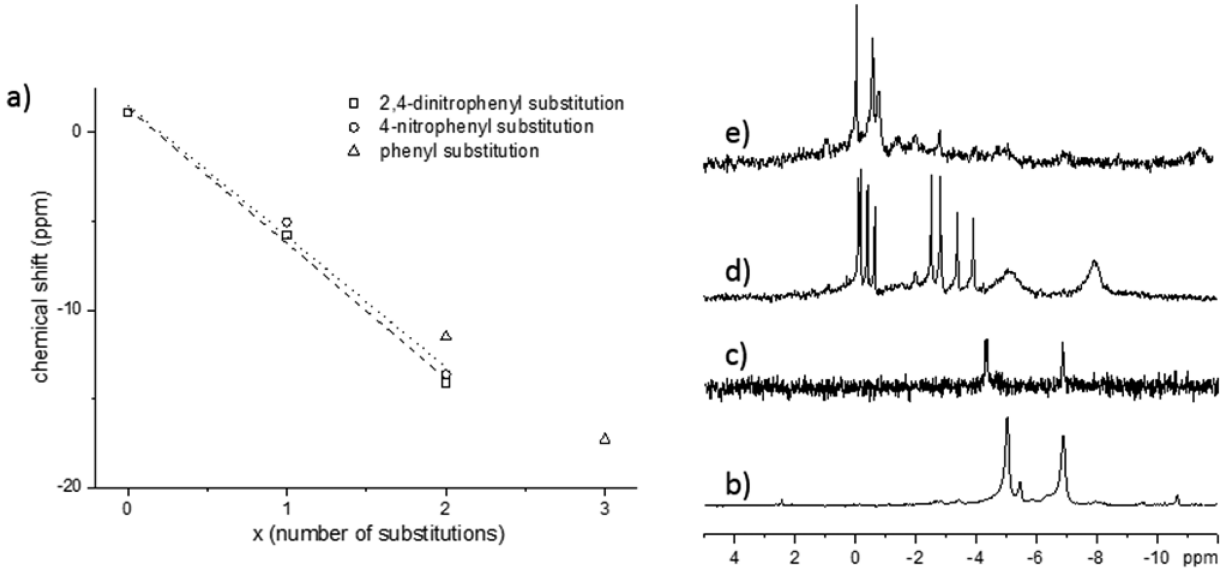

Figure 12. (a) Chemical shifts of ^{31}P NMR resonances for phosphoester substrates $(OP(OH)_{3-x}(OR)_x)$ in water containing CD_3CN vs extent of substitution (x) of phosphoric acid with 2,4-dinitrophenyl, 4-nitrophenyl, and phenyl residues. Comparison of ^{31}P NMR spectra in CD_3CN after addition of DNPP to (b) $[Zn_2(H_2L^3)(OAc)(OH)]^+$, (c) $[Zn_2(H_2L^2)(OAc)_2]^+$, and (d) $[Zn_2(L^4)(OAc)_2]^+$ directly after addition (e) after 48 h.

Table 5. Phosphoester ^{31}P NMR Resonances Obtained before and after Addition of Dizinc(II) Complexes $[Zn_2(H_2L^2)(OAc)_2]^+$, $[Zn_2(H_2L^3)(OAc)(OH)]^+$, and $[Zn_2(L^4)(OAc)_2]^+$

		resonances arising from phosphoesters [ppm]								
$Zn(II)_2$ complex	phospho-ester	metal-free	treated with the $Zn(II)_2$ complexes							
$[Zn_2(H_2L^3)]^{3+}$	PNPP	−5.05	0.62							
$[Zn_2(H_2L^3)]^{3+}$	DNPP	−5.76	−6.85	−5.01	−2.89					
after 14 weeks	DNPP		−6.85	−5.01						
$[Zn_2(H_2L^2)]^{3+}$	DNPP	−5.76	−6.80	−4.25						
after 14 weeks	DNPP		−6.80	−4.25	−2.93					
$[Zn_2(L^4)]^{3+}$	DNPP	−5.76	−3.90	−3.37	−2.81	−2.50	−0.64	−0.40	−0.16	−0.09
after 48 h	DNPP						−0.63			−0.08
$[Zn_2(H_2L^2)]^{3+}$	BDNPP	−14.10								
	0.25eq			−10.25						
	0.5eq			−10.20						
	0.75eq		(−11.46)	−10.22	(−6.88)	(−4.58)				
after 24 h	0.75eq			−10.21	−6.95	−4.54	−1.40			
	1.0eq		−11.40	−10.20	−7.01	−4.48	−1.41			
after 3 weeks	1.0eq				−7.26	−4.45	−1.42			

by a terminal hydroxido group but by the neighboring amide oxygen atom of the supporting dinucleating ligand. The coordination of the bulky PNPP inhibitor in $[Zn_2(H_2L^3)(O_3POC_6H_4NO_2)]PF_6$, compared to the acetate coligand in $[Zn_2(H_2L^3)(OAc)(OH)]PF_6$, leads to an increase of the $Zn^{II}\cdots Zn^{II}$ distance by 0.16 Å, accompanied by the widening of the Zn−O−Zn angle by 6.4°. The structural differences in the dizinc(II) complexes of H_3L^3, $[Zn_2(H_2L^3)(O_3POC_6H_4NO_2)]PF_6$, and $[Zn_2(H_2L^3)(OAc)(OH)]PF_6$ are mainly in the angles within the triangular plane of the trigonal bipyramidal site. Due to the bulkier 4-nitrophenolate residue of PNPP in $[Zn_2(H_2L^3)(O_3POC_6H_4NO_2)]PF_6$, compared to the acetate coligand in $[Zn_2(H_2L^3)(OAc)(OH)]PF_6$, the O(1)−Zn(1)−N(1) angle is widened (136.53(16)° vs 118.77(16)°) and the O(1)−Zn(1)−N(3) angle is contracted (100.50(16)° vs 124.76(15)°). However, the primary coordination sphere of the two complexes is similar. Further investigation of the second coordination sphere in the amide-based complexes $[Zn_2(H_2L^2)(OAc)_2]PF_6$, $[Zn_2(H_2L^3)(OAc)(OH)]PF_6$, $[Zn_2(H_2L^3)(O_3POC_6H_4NO_2)]PF_6$, and $[Zn_2(H_2L^6)(OAc)(OH)]$ indicates that, while the symmetric ligand H_3L^2 forms two hydrogen bonds to the two bridging acetate coligands (one hydrogen bond to each acetate), the symmetric complexes, $[Zn_2(H_2L^3)(OAc)(OH)]PF_6$ and $[Zn_2(H_2L^6)(OAc)(OH)]$, form two hydrogen bonds to the hydroxido ligand, stabilizing this unusual structure. However, the introduction of the monophosphate PNPP, replacing the bridging acetate, leads to the coordination of one of the amide groups, stabilized by hydrogen bonding to the second amide function. The distance between these nitrogen and oxygen atoms of 3.210(6) Å is long compared to the corresponding distances in $[Zn_2(H_2L^2)(OAc)_2]PF_6$, $[Zn_2(H_2L^3)(OAc)(OH)]PF_6$, and $[Zn_2(H_2L^6)(OAc)(OH)]$ (see Table 2). We assume that steric hindrance by the *tert*-butyl groups causes this elongation. Interestingly, no hydrogen bonding to the bridging phosphate, as previously observed with the amino group-containing complex $[Zn_2L^{13}(\mu\text{-PNPP})]^+$ (L^{13} = *N*,*N*-bis(2-pyridylmethyl)-*N*-(6-amino-2-pyridylmethyl)amine), occurs.[10]

dx.doi.org/10.1021/ic5009945 | *Inorg. Chem.* 2014, 53, 9036−9051

^{31}P NMR Studies of Phosphoester Binding. Phosphomonoester Binding. In order to gain further insight into the catalytic mechanism, substrate binding was studied by ^{31}P NMR spectroscopy. ^{31}P NMR spectra of the hexafluoridophosphate salts of the dizinc(II) complexes were measured with 85% H_3PO_4 as an external standard, and the resonance of PF_6 was then used as internal standard for the phosphoester binding experiments. First the phosphoester substrates were measured to study the influence of the ester groups on the ^{31}P chemical shifts (Figure 12a; $NaPF_6$ referenced to −144.30 ppm). Comparison of the ^{31}P shifts in phosphoric acid, PNPP, bis(4-nitrophenyl)phosphate (BPNPP), DNPP, BDNPP, diphenyl phosphate, and triphenyl phosphate shows a linear correlation with the number of protons substituted by phenyl groups in H_3PO_4. Importantly, a comparison of the resonances of the phosphodiesters BDNPP and BPNPP as well as of the phosphomonoesters DNPP and PNPP indicates that the impact of an additional nitro substituent at the phenyl groups is rather small.

The ^{31}P NMR spectrum of the crystallographically investigated complex $[Zn_2(H_2L^3)(O_3POC_6H_4NO_2)]^+$ in acetonitrile has a single resonance at 0.62 ppm, compared to −5.05 ppm for the uncoordinated phosphoester. This effect was also studied using the phosphomonoester DNPP for the four dizinc(II) complexes, in order to gain a deeper understanding of the product-inhibited structure during the BDNPP hydrolysis; the detected resonances are summarized in Table 5.

The spectra recorded after the addition of DNPP to the amine-based complex $[Zn_2(L^4)(OAc)_2]^+$ in deuterated acetonitrile (∼20 vol % water content) show eight resonances shortly after addition (−3.90, −3.37, −2.81, −2.50, −0.64, −0.40, −0.16, and −0.09 ppm) (Figure 12d). Over 48 h further reaction results in the observation of only two resonances, at −0.61 and −0.08 ppm (Figure 12e). A more detailed analysis of the spectrum obtained immediately after addition revealed a pattern of two sets of four resonances, in which always two resonances of the four are separated by about 0.3 ppm (50 Hz) or 0.5 ppm (78 and 85 Hz). ^{31}P NMR studies performed with a series of cyclic phosphates disclosed that, besides the electronegativity effect, the chemical shifts of ^{31}P NMR resonances are also significantly influenced by (i) the O−P−O angle and (ii) the torsional angle R−O−P−O(R) of the phosphate.[35] Therefore, we attribute the eight resonances to four different species (−3.64, −2.66, −0.41, and −0.25 ppm), each of them present in two conformers with varied positions of the dinitrophenyl residue of the phosphoester. After 48 h only the "doublet" at −0.25 ppm remains. The chemical shift difference of 5.51 ppm between the resonances of DNPP in its free form and bound to complex $[Zn_2(L^4)(solv)_x]^{n+}$ is in the same range as found by comparison of free PNPP and $[Zn_2(H_2L^3)(O_3POC_6H_4NO_2)]^+$. Therefore, we propose a similar bridging coordination mode of DNPP to complex $[Zn_2(L^4)(solv)_x]^{n+}$ as found in $[Zn_2(H_2L^3)(O_3POC_6H_4NO_2)]^+$. Once more, it should be emphasized that until this most stable phosphoester-bridged dizinc(II) complex was formed, three different intermediate stages were detectable.

In contrast, when the amido-based complexes $[Zn_2(H_2L^2)(OAc)_2]^+$ and $[Zn_2(H_2L^3)(OAc)(OH)]^+$ dissolved in deuterated acetonitrile (∼3.0 vol % water content for $[Zn_2(H_2L^2)(OAc)_2]^+$ and ∼1.2 vol % water content for $[Zn_2(H_2L^3)(OAc)(OH)]^+$) were treated with 1 equiv of DNPP, two major resonances with similar chemical shifts appeared in the ^{31}P NMR spectra (−6.85, −5.01 ppm and −6.80, −4.25 ppm) (Figure 12b,c). Therefore, we assume similar coordination modes of DNPP to $[Zn_2(H_2L^2)(solv)_x]^{n+}$ and $[Zn_2(H_2L^3)(solv)_x]^{n+}$. Moreover, the resonances detected were downfield and upfield shifted, respectively, compared to the free phosphomonoester. The extent of the shifts (0.75 to 1.51 ppm) is small compared to the cases discussed above. This suggests a rather different coordination mode of DNPP to $[Zn_2(H_2L^2)(solv)_x]^{n+}$ and $[Zn_2(H_2L^3)(solv)_x]^{n+}$ than observed in the X-ray structure of $[Zn_2(H_2L^3)(O_3POC_6H_4NO_2)]^+$. Studies with cyclic phosphoesters have shown that the O−P−O angle has a significant impact on the ^{31}P NMR chemical shift.[35] For example, an increase in the bond angle of phosphotriesters results in the better shielding of the phosphorus atom and therefore in an upfield shift of the ^{31}P NMR resonance. Assuming the same binding mode for DNPP and PNPP, an upfield shift due to a larger O−P−O angle in the case of DNPP competes with a downfield shift due to coordination to two Zn^{II} ions, and this could explain the smaller extent of the downfield shifts in the cases of DNPP with $[Zn_2(H_2L^2)(OAc)_2]^+$ and $[Zn_2(H_2L^3)(OAc)(OH)]^+$. The major resonances at around −6.8 and −4 to −5 ppm can be attributed either to a complex structure with two DNPP ligands in two different electronic environments or to two different complex structures, each of them containing only one bound DNPP. Although the two major resonances upon binding DNPP by the amide-based complexes $[Zn_2(H_2L^2)(solv)_x]^{n+}$ and $[Zn_2(H_2L^3)(solv)_x]^{n+}$ are similar, their ^{31}P NMR spectra are different: while the third resonance at −2.89 ppm was detected immediately after addition of DNPP to $[Zn_2(H_2L^3)(OAc)(OH)]^+$ and disappears after 14 weeks, a species with a similar signal was not observed with $[Zn_2(H_2L^2)(OAc)_2]^+$ but when a spectrum was measured after 14 weeks (−2.93 ppm). This implies that both complexes form different species with DNPP in different coordination modes, but the equilibrium constants are dependent on the symmetry of the complex backbone. This could explain the different catalytic activity of the complexes $[Zn_2(H_2L^2)(OAc)_2]^+$ and $[Zn_2(H_2L^3)(OAc)(OH)]^+$.

Phosphodiester Binding. The binding of BDNPP was investigated for the most active complex $[Zn_2(H_2L^2)(OAc)_2]^+$ by stepwise addition of 0.25 equiv of the phosphodiester and recording the ^{31}P NMR spectra at each step (∼1.0 vol % water content) (Figure 13). Addition up to 0.5 equiv of BDNPP to a solution of the complex in CD_3CN resulted in the formation of only one phosphorus-containing species with a ^{31}P NMR resonance at −10.22 ppm (Figure 13b,c), in addition to free BDNPP with a resonance at −14.43 ppm (Figure 13a). After further addition of BDNPP two additional signals at −6.86 and −4.58 ppm occurred in the ^{31}P NMR spectrum, and the signal integration increases upon increase of BDNPP concentration. Further reaction led to the disappearance of the initially detected species and formation of a new species with a resonance at −1.41 ppm.

Comparison with the spectra monitored after addition of the phosphomonoester DNPP to $[Zn_2(H_2L^2)(OAc)_2]^+$ (Figure 12c) allows to assign the resonances at −6.86 and −4.58 ppm to species containing DNPP. The increase of the integrals of these two species is accompanied by the decrease of the initially detected resonance at −10.22 ppm. Therefore, we suggest that the resonance at −10.22 ppm originates from a BDNPP−complex adduct. It follows that the binding of the phosphodiester to the Zn^{II} ion leads to a downfield shift by

dx.doi.org/10.1021/ic5009945 | Inorg. Chem. 2014, 53, 9036−9051

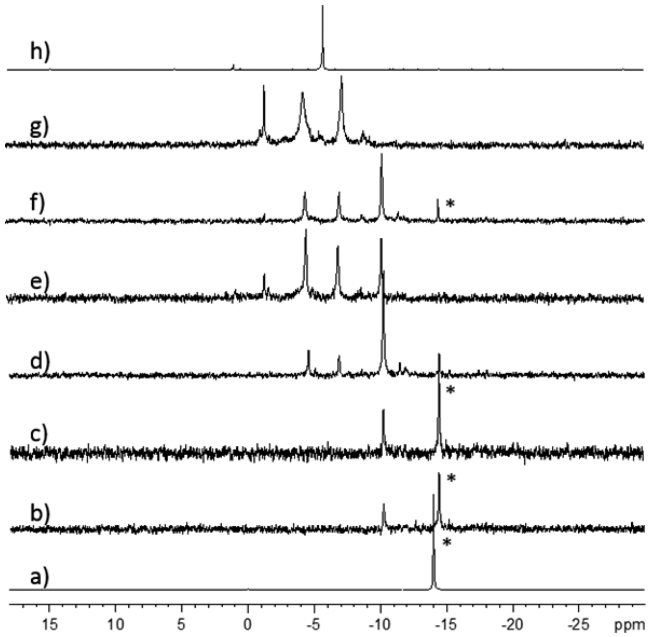

Figure 13. ^{31}P NMR measurements upon addition of BDNPP to $[Zn_2(H_2L^2)(OAc)_2]^+$ in CD_3CN: (a) BDNPP reference, (b) 0.25 equiv of BDNPP, (c) 0.5 equiv of BDNPP, (d) 0.75 equiv of BDNPP, (e) 0.75 equiv of BDNPP after 24 h, (f) 1.0 equiv of BDNPP, (g) 1.0 equiv of BDNPP after 16 days, and (h) DNPP reference (* unreacted BDNPP).

4.2 ppm compared to free BDNPP, accompanied by the activation of the phosphodiester BDNPP. The following hydrolysis of BDNPP provides the phosphomonoester DNPP, which binds in the same way as by direct addition of DNPP to the complex. The decrease of the signal assigned to the BDNPP–complex adduct is accompanied by an increase of a signal at −1.41 ppm. Although the structure of the corresponding species remains unclear, we speculate that this complex adduct is able to release the DNPP product and therefore continues to catalyze the BDNPP hydrolysis.

CONCLUSION

The four phosphatase models $[Zn_2(L^1)(OAc)_2]^+$, $[Zn_2(H_2L^2)(OAc)_2]^+$, $[Zn_2(H_2L^3)(OAc)(OH)]^+$, and $[Zn_2(L^4)(OAc)_2]^+$ with no substituents, two symmetrically disposed and two asymmetrically disposed amides or two asymmetrically disposed amine anchor groups for hydrogen bonding, respectively, lead to strikingly different structures of the dizinc(II) complexes and their adducts with the phosphoester substrates and their hydrolysis products. NMR spectroscopy indicates that the solution structures of the two complexes built up by an asymmetric ligand backbone contain two unequal Zn^{II} centers. Interestingly, in $[Zn_2(H_2L^3)(OAc)(OH)]^+$, the asymmetry of the ligand with respect to the amide groups leads to two strikingly different Zn^{II} sites, one being six- and one five-coordinate, and the former site exhibiting a rare example with a Zn^{II}–OH bond. The main impact of the secondary interactions is shown to be reduced stability of the catalyst–substrate and catalyst–inhibitor (hydrolysis product) adducts, and this obviously depends on the hydrogen-bonding sites (symmetric vs asymmetric arrangement) and the type of hydrogen donor group. Moreover, the impact of the hydrogen bond donors of the catalyst on their hydrolytic activity is clearly pH dependent. For the zinc(II)-based phosphatase mimics, it appears that at pH = 7 the asymmetrical amine-based system $[Zn_2(L^4)(OAc)_2]^+$ is the most efficient due to an increased substrate affinity imposed by hydrogen bonding, while at pH = 9.5 and pH = 11, the symmetric, sterically hindered, amide-based system $[Zn_2(H_2L^2)(OAc)_2]^+$ is more efficient, and this is primarily due to less stable catalyst–inhibitor complexes.

EXPERIMENTAL SECTION

Materials and Methods. Nuclear magnetic resonance (NMR) spectra were carried out with Bruker AV400 and AV500 instruments. The spectra were conducted in CD_3OD or CD_3CN. Chemical shifts of ^{1}H and ^{13}C NMR spectra are reported in ppm, relative to known solvent peak references. For ^{31}P NMR spectra 85% phosphoric acid was used as the external reference. Two-dimensional correlation spectroscopy (COSY), nuclear Overhauser-effect spectroscopy (NOESY), heterodinuclear single quantum correlation (HSQC), and hetereodinuclear multiple-bond connectivity (HMBC) experiments were used to assign each signal in the spectra. The following abbreviations were used: s (singlet), bs (broad singlet), d (doublet), dd (doublet of doublets), ddd (doublet of doublets of doublets), t (triplet), dt (doublet of triplets), sep (septet), and m (multiplet). Coupling constants are given in Hz. High-resolution mass spectra were collected with a Bruker microTOFQ ESI-MS spectrometer by Mr. Graham Macfarlane at the University of Queensland and processed with Bruker Compass Data Analysis 4.0 software. FT-infrared spectroscopy was carried out with a PerkinElmer SPECTRUM 2000 FT-IR spectrometer with a Smiths DuraSamplIR II ATR diamond window. Elemental microanalyses were performed in the analytic laboratories of the Institute of Chemistry at the University of Heidelberg with an Elementar Vario EL machine. X-ray crystallographic data were collected with an Oxford Diffraction Gemini Ultra dual source CCD diffractometer. The structures were solved by direct methods using the SHELXS computer program and refined by the full-matrix least-squares method, with the SHELXL97 computer program.[36,37]

Synthesis of Ligands and Complexes. Ligand HL^1,[15,16] ligand H_3L^2,[13] bis(pyridin-2-ylmethyl)amine (**1**),[38] 2-(((pyridin-2-ylmethyl)-amino)methyl)phenol (**1a**),[39] 3-(chloromethyl)-2-hydroxy-5-methyl-benzaldehyde (**2**),[40,41] 3-((bis(pyridin-2-ylmethyl)amino)methyl)-2-hydroxy-5-methylbenzaldehyde (**3**),[42] 2-hydroxy-3-(((2-hydroxybenzyl)(pyridin-2-ylmethyl)amino)methyl)-5-methylbenzaldehyde (**3a**),[43] and *N*,*N*-bis((2-pivaloylamidopyridin-6-yl)methyl)amine (**4**)[44] were prepared as described previously with minor modifications. For comparison reasons the analysis data of the ligands HL^1 and H_3L^2 are given additionally.

HL^1. ^{1}H NMR (CD_3CN, 500.13 MHz): 2.18 (s, 3H, *H*17), 3.68 (s, 4H, *H*13, *H*21), 3.76 (s, 8H, *H*6, *H*12, *H*27, *H*33), 6.96 (s, 2H, *H*15, *H*18), 7.15 (ddd, 4H, ^3J = 7.52 Hz, ^3J = 4.95 Hz, ^4J = 1.10 Hz, *H*2, *H*8, *H*23, *H*29), 7.44 (d, 4H, ^3J = 7.70 Hz, *H*4, *H*10, *H*25, *H*31), 7.62 (td, 4H, ^3J = 7.70 Hz, ^4J =1.83 Hz, *H*3, *H*9, *H*24, *H*30), 8.45 (ddd, 4H, ^3J = 4.77 Hz, ^3J = 4.77 Hz, ^4J = 1.00 Hz, *H*1, *H*7, *H*22, *H*28) ppm. ^{13}C NMR (CD_3CN, 100.62 MHz): 20.58 (*C*17), 55.34 (*C*13, *C*21), 60.26 (*C*6, *C*12, *C*27, *C*33), 123.01 (*C*2, *C*8, *C*23, *C*29), 123.88 (*C*4, *C*10, *C*25, *C*31), 124.85 (*C*14, *C*19), 128.08 (*C*16), 130.84 (*C*15, *C*18), 137.43 (*C*3, *C*9, *C*24, *C*30), 149.73(*C*1, *C*7, *C*22, *C*28), 150.66 (*C*20), 160.16 (*C*5, *C*11, *C*26, *C*32) ppm. FT-IR spectroscopy (ν, cm^{-1}): 3063 (ν(Ar–H)), 3011 (ν(Ar–H)), 2924 (ν(C–H)), 2828 (ν(C–H)), 1590 (ν(C=C)), 1569 (ν(C=C)), 1475 (ν(C=C)), 1433 (ν(C=C)), 754 (δ(py-H)). HRMS (ESI$^+$, CH_3CN): *m*/*z* 729.424 ($[C_{43}H_{53}N_8O_3]^+$, 729.424). HRMS (ESI$^+$, CH_3CN): *m*/*z* 531.287 ($[C_{33}H_{35}N_6O]^+$, 531.287).

H_3L^2. ^{1}H NMR (CD_3CN, 500.13 MHz): 1.24 (s, 18H, *H*36, *H*39), 2.21 (s, 3H, *H*17), 3.72 (s, 4H, *H*13, *H*21), 3.75 (s, 4H, *H*27, *H*33), 3.78 (s, 4H, *H*6, *H*12), 7.04 (s, 2H, *H*15, *H*18), 7.15 (m,4H, *H*2, *H*8, *H*25, *H*31), 7.46 (d, 2H, ^3J = 8.07 Hz, *H*4, *H*10), 7.62 (td, 2H, ^3J = 7.70 Hz, ^4J = 1.83 Hz, *H*3, *H*9), 7.64 (t, 2H, ^3J = 7.89 Hz, *H*24, *H*30), 7.97 (d, 2H, ^3J = 8.44 Hz, *H*23, *H*29), 8.28 (bs, 2H, N*H*), 8.44 (ddd, 2H, ^3J = 5.14 Hz, ^3J = 4.04 Hz, ^4J = 0.90 Hz, *H*1, *H*7) ppm. ^{13}C NMR ($CDCl_3$, 100.55 MHz): 20.60 (*C*17), 27.45 (*C*36, *C*39), 39.75 (*C*35,

dx.doi.org/10.1021/ic5009945 | Inorg. Chem. 2014, 53, 9036–9051

C38), 54.72 (C13, C21), 58.97 (C27, C33), 59.88 (C6, C12), 111.69 (C23, C29), 117.97 (C25, C31), 121.91 (C2, C8), 122.71 (C4, C10), 123.84 (C14, C19), 127.63 (C16), 129.65 (C15, C18), 136.51 (C3, C9), 138.86 (C24, C30), 148.73 (C1, C7), 150.97 (C22, C28), 153.08 (C20), 157.28 (C26, C32), 159.37 (C5, C11), 177.13 (C34, C37) ppm. FT-IR spectroscopy (ν, cm^{-1}): 3438 (ν(N−H)), 3389 (ν(O−H)), 2964 (ν(C−H)), 2869 (ν(C−H)), 2817 (ν(C−H)), 1686 (ν(C═O)), 1523 (ν(C−N), δ(CNH)), 1405 (ν(C−$(CH_3)_3$), 797 (δ(py−H)). HRMS (ESI^+, CH_3CN): m/z 729.424 ($[C_{43}H_{53}N_8O_3]^+$, 729.424). Anal. (%) Calcd for $C_{43}H_{52}N_8O_3{\cdot}CH_3OH$: C 69.45, H 7.42, N 14.73;. Found: C 69.47, H 7.10, N 14.98.

H_3L^3. Molecular sieves (4 Å) were added to a solution of **3** (3.13 g, 9.0 mmol) in anhydrous CH_2Cl_2 (23 mL), followed by the dropwise addition of a solution of **4** (3.58 g, 9.0 mmol) in anhydrous CH_2Cl_2 (10 mL). The mixture was stirred for 3 h at room temperature. Afterward the solution was treated with sodium triacetoxyborohydride (4.20 g, 19.8 mmol) by addition in portions, and the mixture stirred at room temperature overnight. The reaction was quenched by addition of saturated sodium bicarbonate solution (30 mL) and stirring for 45 min. The pH was subsequently adjusted to 8 by addition of solid sodium carbonate. The phases were separated, and the aqueous phase was extracted three times with CH_2Cl_2 (30 mL). The combined organic phases were washed with saturated sodium carbonate solution (20 mL) and brine (20 mL) and dried over sodium sulfate. Removal of solvent under reduced pressure gave a brownish foam. Purification by column chromatography (SiO_2, DEE/NH_3 in MeOH (7 N), 98:2, R_f = 0.48) yielded H_3L^3 as a white solid (1.94 g, 30%). ^{1}H NMR (CD_3CN, 500.13 MHz): 1.25 (s, 18H, *H*36, *H*39), 2.21 (s, 3H, *H*17), 3.69 (s, 2H, *H*21), 3.73 (s, 4H, *H*27, *H*33), 3.74 (s, 2H, *H*13), 3.79 (s, 4H, *H*6, *H*12), 6.88 (ds, 1H, ^4J = 1.74 Hz, *H*18), 7.10 (d, 2H, ^3J = 8.06 Hz, *H*25, *H*31), 7.15 (ds, 1H, ^4J = 0.92 Hz, *H*15), 7.15 (ddd, 2H, ^3J = 7.28 Hz, ^3J = 6.22 Hz, ^4J = 1.06 Hz, *H*2, *H*8), 7.50 (d, 2H, ^3J = 8.07 Hz, *H*4, *H*10), 7.62 (t, 2H, ^3J = 8.44 Hz, *H*24, *H*30), 7.64 (dt, 2H, ^3J = 7.70 Hz, ^4J = 1.83 Hz, *H*3, *H*9), 7.96 (d, 2H, ^3J = 8.44 Hz, *H*23, *H*29), 8.28 (bs, 2H, N*H*), 8.46 (ddd, 2H, ^3J = 6.60 Hz, ^3J = 4.77 Hz, ^4J = 1.10 Hz, *H*1, *H*7) ppm. ^{13}C NMR (CD_3CN, 100.61 MHz): 20.77 (C17), 27.68 (C36, C39), 40.51 (C35, C38), 54.35 (C13), 56.33 (C21), 59.59 (C27, C33), 60.75 (C6, C12), 112.49 (C23, C29), 119.19 (C25, C31), 123.06 (C2, C8), 123.76 (C4, C10), 124.72 (C19), 125.64 (C14), 128.49 (C16), 130.71 (C15), 130.95 (C18), 137.44 (C3, C9), 139.86 (C24, C30), 149.88 (C1, C7), 152.29 (C22, C28), 154.37 (C20), 158.66 (C26, C32), 160.60 (C5, C11), 177.93 (C34, C37) ppm. FT-IR spectroscopy (ν, cm^{-1}): 3438 (ν(N−H)), 3389 (ν(O−H)), 2964 (ν(C−H)), 2869 (ν(C−H)), 2817 (ν(C−H)), 1687 (ν(C═O)), 1517 (ν(C−N), δ(CNH)), 1403 (ν(C−$(CH_3)_3$), 798 (δ(py−H)). HRMS (ESI^+, CH_3CN): m/z 729.424 ($[C_{43}H_{53}N_8O_3]^+$, 729.424). Anal. (%) Calcd for $C_{43}H_{52}N_8O_3$: C 70.85, H 7.19, N 15.37. Found: C 70.63, H 7.06, N 15.29.

HL^4. A solution of H_3L^3 (300.0 mg, 0.41 mmol) in ethanol (10.0 mL) was treated with aqueous sodium hydroxide solution (6 M, 2 mL), after which the mixture was heated at 70 °C for 3 days while stirring. Subsequently the solvent was removed under reduced pressure, and the remaining solid taken up in water (10 mL). Concentrated hydrochloric acid was added until the pH reached 1, and the pH was subsequently adjusted to 7 using saturated sodium bicarbonate solution. After the product was extracted into CH_2Cl_2 (3 × 10 mL) the combined organic phases were washed with saturated sodium bicarbonate solution (10 mL) and dried over sodium sulfate. Removal of the solvent yielded a crude product, which was purified by column chromatography ($Alox_{neutral}$, MeOH), yielding the desired product HL^4 as a white solid (108.8 mg, 47%). ^{1}H NMR (CD_3CN, 500.13 MHz): 2.18 (s, 3H, *H*17), 3.51 (s, 4H, *H*27, *H*33), 3.57 (s, 2H, *H*21), 3.70 (s, 2H, *H*13), 3.77 (s, 4H, *H*6, *H*12), 6.35 (d, 2H, ^3J = 8.07 Hz, *H*23, *H*29), 6.61 (d, 2H, ^3J = 6.97 Hz, *H*25, *H*31), 6.88 (s, 1H, *H*18), 6.95 (s, 1H, *H*15), 7.17 (ddd, 2H, ^3J = 6.24 Hz, ^3J = 5.14 Hz, ^4J = 1.10 Hz, *H*2, *H*8), 7.33 (t, 2H, ^3J = 7.70 Hz, *H*24, *H*30), 7.46 (d, 2H, ^3J = 7.70 Hz, *H*4, *H*10), 7.66 (td, 2H, ^3J = 7.70 Hz, ^4J = 1.83 Hz, *H*3, *H*9), 8.48 (d, 2H, ^3J = 5.14 Hz, *H*1, *H*7) ppm. ^{13}C NMR (CD_3CN, 100.61 MHz): 20.47 (C17), 52.51 (C13), 54.96 (C21), 60.20 (C27, C33), 60.54 (C6, C12), 107.83 (C23, C29), 113.09 (C25, C31), 123.24 (C2, C8), 124.26 (C4, C10), 124.72 (C14), 124.99 (C19), 131.20 (C15), 131.39 (C18), 137.74 (C3, C9), 139.16 (C24, C30), 149.87 (C1, C7), 157.85 (C26, C32), 160.01 (C5/C11/C22/C28), 160.28 (C5/C11/C22/C28) ppm. FT-IR spectroscopy (ν, cm^{-1}): 3322 (ν(N−H)), 3199 (ν (N−H)), 3059 (ν(Ar−H)), 3011 (ν(Ar−H)), 2917 (ν(C−H)), 2816 (ν(C−H)), 1594 (ν(C═C)), 1574 (ν(C═C)), 1466 (ν(C═C)), 1435 (ν(C═C)), 1299 (ν(C−N)), 1221 (ν(C−N)), 758 (δ(py-H)). HRMS (ESI^+, CH_3CN): m/z 561.308 ($[C_{33}H_{37}N_8O]^+$, 561.309).

H_4L^6. A solution of **3a** (3.56 g, 9.8 mmol) in anhydrous CH_2Cl_2 (25 mL) was treated with molecular sieves (4 Å) before a solution of **4** (4.10 g, 10.3 mmol) in anhydrous CH_2Cl_2 (11 mL) was added dropwise. After the mixture was stirred for 3 h at room temperature sodium triacetoxyborohydride (4.59 g, 21.7 mmol) was added in small portions, and the reaction mixture left to react at room temperature while stirring. The reaction was quenched by addition of saturated sodium bicarbonate solution (30 mL) and stirring for 45 min before the pH was adjusted to 8 by addition of solid sodium carbonate. The phases were separated, and the aqueous phase was extracted three times with CH_2Cl_2 (30 mL). The combined organic phases were washed with saturated sodium carbonate solution (20 mL) and brine (20 mL) and dried over sodium sulfate. Removal of solvent under reduced pressure gave an orange foam. Purification by column chromatography (SiO_2, DEE/*n*-hexane/NH_3 in MeOH (7 N), 90:8:2, R_f = 0.57) yielded H_4L^6 as a white solid (4.50 g, 62%). ^{1}H NMR (CD_3CN, 500.13 MHz): 1.26 (s, 18H, *H*36, *H*39), 2.16 (s, 3H, *H*17), 3.69 (s, 2H, *H*21), 3.74 (s, 4H, *H*27, *H*33), 3.75 (s, 2H, *H*13), 3.76 (s, 2H, *H*6), 3.78 (s, 2H, *H*12), 6.74 (m, 2H, *H*7, *H*9), 6.85 (sd, 1H, ^4J = 1.83 Hz, *H*18), 6.99 (sd, 1H, ^4J = 1.47 Hz, *H*15), 7.05 (d, 3H, ^3J = 7.34 Hz, *H*10, *H*25, *H*31), 7.11 (td, 1H, ^3J = 7.70 Hz, ^4J = 1.83 Hz, *H*8), 7.14 (d, 1H, ^3J = 7.70 Hz, *H*4), 7.19 (ddd, 1H, ^3J = 7.70 Hz, ^3J = 6.60 Hz, ^4J = 1.10 Hz, *H*2), 7.58 (td, 1H, ^3J = 7.70 Hz, ^4J = 1.83 Hz, *H*3), 7.61 (t, 2H, ^3J = 7.70 Hz, *H*24, *H*30), 7.97 (d, 2H, ^3J = 7.70 Hz, *H*23, *H*29), 8.33 (bs, 2H, N*H*), 8.52 (ddd, 1H, ^3J = 5.14 Hz, ^3J = 4.03 Hz, ^4J = 0.73 Hz, *H*1) ppm. ^{13}C NMR (CD_3CN, 100.61 MHz): 20.62 (C17), 27.70 (C36, C39), 40.53 (C35, C38), 53.17 (C13), 57.22 (C21), 57.85 (C12), 59.28 (C27, C33), 59.36 (C6), 112.58 (C23, C29), 116.92 (C9), 119.12 (C25, C31), 119.85 (C7), 123.33 (C2), 124.14 (C11), 124.44 (C4), 124.53 (C14/C19), 124.85 (C14/C19), 128.71 (C16), 129.72 (C8), 130.84 (C10), 131.28 (C18), 131.55 (C15), 137.67 (C3), 139.99 (C24, C30), 149.86 (C1), 152.37 (C22, C28), 154.51 (C20), 158.22 (C26, C32), 158.84 (C5/C11), 158.93 (C5/C11), 177.96 (C34, C37) ppm. FT-IR spectroscopy (ν, cm^{-1}): 3392 (ν(N−H)), 2968 (ν(C−H)), 2870 (ν(C−H)), 2824 (ν(C−H)), 1689 (ν(C═O)), 1522 (ν(C−N), δ(CNH)), 1450 (ν(C−$(CH_3)_3$), 751 (δ(py−H)). HRMS (ESI^+, CH_3CN): m/z 744.421 ($[C_{44}H_{54}N_7O_4]^+$, 744.423). Anal. (%) Calcd for $C_{43}H_{52}N_8O_3$: C 71.04, H 7.18, N 13.18. Found: C 71.11, H 7.26, N 12.93.

Synthesis of Dinuclear Zn^{II} Complexes. The ligand (0.137 mmol) was dissolved in methanol (5 mL), and sodium hydroxide solution (2 M, 69 μL) was added. After addition of $Zn^{II}(OAc)_2$ acetate (57.8 mg, 0.274 mmol) the mixture was heated to 50 °C for 20 min. Sodium hexafluoridophosphate (46.0 mg, 0.274 mmol) was added to the hot solution. The compounds were obtained as colorless crystals upon standing, and these were collected by filtration.

$[Zn_2(L^1)(OAc)_2]PF_6$ (102.5 mg, 81%). ^{1}H NMR (CD_3CN, 500.13 MHz): 1.95 (s, 3H, *H*17), 1.99 (s, 6H, *H*2a, *H*4a), 3.17 (d, 2H, ^2J = 11.37 Hz, *H*13), 3.35 (d, 2H, ^2J = 16.51 Hz, *H*12, *H*33), 3.48 (d, 2H, ^2J = 16.14 Hz, *H*12, *H*33), 3.88 (d, 2H, ^2J = 11.37 Hz, *H*13), 3.97 (d, 2H, ^2J = 14.31 Hz, *H*6, *H*27), 4.50 (d, 2H, ^2J = 14.31 Hz, *H*6, *H*27), 6.40 (s, 2H, *H*15, *H*18), 6.44 (d, 2H, ^3J = 7.70 Hz, *H*10, *H*31), 7.01 (dd, 2H, ^3J = 7.34 Hz, ^3J = 5.14, *H*8, *H*29), 7.29 (td, 2H, ^3J = 7.70 Hz,, ^4J = 1.47 Hz, *H*9, *H*30), 7.43 (dd, 2H, ^3J = 7.34 Hz, ^3J = 5.14 Hz, *H*2, *H*23), 7.48 (d, 2H, ^3J = 8.07 Hz, *H*4, *H*25), 7.92 (td, 1H, ^3J = 7.79 Hz, ^4J = 1.65 Hz, *H*3, *H*24), 8.24 (d, 2H, ^3J = 4.774 Hz, *H*7, *H*28), 8.76 (d, 2H, ^3J = 4.40 Hz, *H*1, *H*22) ppm. ^{13}C NMR (CD_3CN, 100.61 MHz): 20.15 (C17), 24.91 (C35), 58.50 (C12, C33), 60.67 (C13, C21), 60.76 (C6, C27), 121.94 (C10, C31), 123.63 (C8, C29), 124.32 (C14, C19), 124.95 (C2, C23), 125.08 (C16), 125.18 (C4, C25), 131.90 (C15, C18), 138.60 (C9, C30), 140.30 (C3, C24), 147.18 (C7, C28), 148.58

dx.doi.org/10.1021/ic5009945 | *Inorg. Chem.* 2014, 53, 9036−9051

(C1, C22), 155.83 (C11, C32), 156.30 (C5, C26), 160.22 (C20), 179.27 (C34) ppm. FT-IR spectroscopy (ν, cm^{-1}): 2996 (ν(C−H)), 2931 (ν(C−H)), 2844 (ν(C−H)), 1600 (ν_a(OAc)), 1406 (ν_s(OAc)), 831 (ν(P−F)), 650 (δ(py-H)), 556 (δ(F−P−F)). HRMS (ESI^+, CH_3CN): m/z 360.070 ($[C_{35}H_{36}N_6O_3Zn_2]^{2+}$, 360.069); 765.138 ($[C_{36}H_{37}N_6O_5Zn_2]^+$, 765.136). HRMS ($ESI^+$, CH_3OH): m/z 779.154 ($[C_{37}H_{39}N_6O_5Zn_2]^+$, 779.153). Anal. (%) Calcd for $C_{37}H_{39}N_6O_5PF_6Zn_2$: C 48.10, H 4.26, N 9.11. Found: C 48.10, H 4.50, N 9.11.

$[Zn_2(H_2L^2)(OAc)_2]PF_6$ (116.6 mg, 76%). ^1H NMR (CD_3CN, 500.13 MHz): 1.27 (s, 18H, H36, H39), 1.91 (s, 3H, H17), 2.12 (s, 6H, H2a, H4a), 3.19 (d, 2H, ^2J = 11.37 Hz, H13, H21),3.42−3.56 (m, 4H, H6, H12), 3.82 (d, 2H, ^2J = 11.74 Hz, H13, H21), 3.97 (d, 2H, ^2J = 15.04 Hz, H27, H33), 4.59 (d, 2H, ^2J = 15.04 Hz, H27, H33), 6.40 (s, 2H, H15, H18), 6.59 (d, 2H, ^3J = 7.70 Hz, H4, H10), 7.05 (dd, 2H, ^3J = 6.79 Hz, ^3J = 6.05 Hz, H2, H8), 7.16 (d, 2H, ^3J = 7.70 Hz, H25, H31), 7.38 (td, 2H, ^3J = 7.70 Hz, ^4J = 1.47 Hz, H3, H9), 7.85 (t, 2H, ^3J = 7.70 Hz, H24, H30), 8.14 (d, 2H, ^3J = 8.44 Hz, H23, H29), 8.39 (m, 2H, H1, H7), 9.89 (s, 2H, NH) ppm. ^{13}C NMR (CD_3CN, 100.61 MHz) 19.16 (C17), 25.25 (C2a, C4a) 26.65 (C36, C39), 39.82 (C35, C38), 57.10 (C6, C12), 60.16 (C13, C21), 61.12 (C27, C33), 115.87 (C23, C29), 119.07 (C25, C31), 121.74 (C4, C10), 122.87 (C2/C8/C14/C19), 122.94 (C2/C8/C14/C19), 124.74 (C16), 130.42 (C15, C18), 138.89 (C3, C9), 141.03 (C24, C30), 146.22 (C1, C7), 151.98 (C22, C28), 154.39 (C26, C32), 155.14 (C5, C11), 158.96 (C20), 177.81 (C34, C37), 178.89 (C1a, C3a) ppm. ^{31}P NMR (CD_3CN, 100.61 MHz): −144.29 (sep, PF_6^-) ppm. FT-IR spectroscopy (ν, cm^{-1}): 3293 (ν(N−H)), 2976 (ν(C−H)), 2924 (ν(C−H)), 2877 (ν(C−H)), 1700 (ν(C═O)), 1600 (ν_a(OAc)), 1536 (ν(C−N), δ(CNH)), 1458 (ν(C−$(CH_3)_3$), 1406 (ν_s(OAc)), 1277 (ν(C−N)), 841 (ν(P−F)), 650 (δ(py−H)), 557 (δ(F−P−F)). HRMS (ESI^+, CH_3CN): m/z 429.128 ($[C_{43}H_{50}N_8O_3Zn_2]^{2+}$, 429.127). HRMS ($ESI^+$, CH_3OH): m/z 977.295 ($[C_{47}H_{57}N_8O_7Zn_2]^+$, 977.293). Anal. (%) Calcd for $C_{47}H_{57}N_8O_7PF_6Zn_2$: C 50.32, H 5.12, N 9.99. Found: C 50.09, H 5.26, N 9.96.

$[Zn_2(H_2L^3)(OAc)(OH)]PF_6$ (23.2 mg, 16%). ^1H NMR (CD_3CN, 500.13 MHz): 0.85 (s, 9H, H36/H39), 1.35 (s, 9H, H36/H39), 1.99 (s, 3H, H17), 2.03 (s, 3H, H2a), 3.36 (d, 1H, ^2J = 11.74 Hz, H13), 3.40 (d, 1H, ^2J = 11.74 Hz, H21), 3.56 (d, 1H, ^2J = 15.77 Hz, H27), 3.67 (d, 1H, ^2J = 15.41 Hz, H27), 3.78 (d, 1H, ^2J = 16.87 Hz, H12), 3.84 (d, 1H, ^2J = 17.24 Hz, H12), 3.92 (d, 1H, ^2J = 14.31 Hz, H33), 4.03 (d, 1H, ^2J = 11.37 Hz, H13), 4.12−4.21 (m, 2H, H6, H21), 4.28 (d, 1H, ^2J = 17.97 Hz, H6), 4.38 (d, 1H, ^2J = 14.31 Hz, H33), 6.29 (d, 1H, ^3J = 7.34 Hz, H25), 6.61 (sd, ^4J = 1.83 Hz, H15), 6.64 (sd, ^4J = 1.83 Hz, H18), 7.10 (d, 1H, ^3J = 7.70 Hz, H31), 7.14 (d, 1H, ^3J = 7.70 Hz, H10), 7.25 (dd, 1H, ^3J = 8.44 Hz, ^3J = 7.70 Hz, H24), 7.36 (dd, 1H, ^3J = 6.20 Hz, H8), 7.53 (d, 1H, ^3J = 8.07 Hz, H4), 7.60 (dd, 1H, ^3J = 6.20 Hz, H2), 7.80 (td, 1H, ^3J = 7.79 Hz, ^4J = 1.65 Hz, H9), 7.81−7.87 (m, 2H, H23, H30), 8.08 (td, 1H, ^3J = 7.79 Hz, ^4J = 1.65 Hz, H3), 8.33 (d, 1H, ^3J = 8.44 Hz, H29), 8.59 (d, 1H, ^3J = 4.77 Hz, H7), 8.80 (d, 1H, ^3J = 5.14 Hz, H1) ppm. ^{13}C NMR (CD_3CN, 125.76 MHz): 20.18 (C17), 27.80 (C16/C39), 27.87 (C16/C39), 40.54 (C35/C38), 41.24 (C35/C38), 57.74 (C12), 58.87 (C13), 59.86 (C27), 61.29 (C33), 61.38 (C6), 61.69 (C21), 114.57 (C23), 115.74 (C29), 117.72 (C25), 119.15 (C31), 124.67(C10/C14), 124.73 (C10/C14), 125.03 (C4), 125.25 (C8/C19), 125.29 (C8/C19), 126.10 (C2), 127.42 (C16), 133.16 (C18), 133.42 (C15), 139.92 (C24), 141.43 (C30), 141.65 (C9), 142.62 (C3), 149.07 (C7), 149.77 (C1), 153.42 (C22/C28), 153.72 (C26), 154.29 (C32), 155.05 (C22/C28), 156.56 (C5), 157.12 (C11), 160.00 (C20), 179.60 (C34/C37), 179.64 (C34/C37), 180.66 (C1a) ppm. ^{31}P NMR (CD_3CN, 100.61 MHz): −144.29 (sep, PF_6^-) ppm. FT-IR spectroscopy (ν, cm^{-1}): 2982 (ν(C−H)), 2937 (ν(C−H)), 2876 (ν(C−H)), 1687 (ν(C═O)), 1581 (ν_a(OAc)), 1545 (ν(C−N), δ(CNH)), 1461 (ν(C−$(CH_3)_3$), 1442 (ν_s(OAc)), 1306 (ν(C−N)), 834 (ν(P−F)), 650 (δ(py-H)), 556 (δ(F−P−F)). HRMS (ESI^+, CH_3CN): m/z 429.130 ($[C_{43}H_{50}N_8O_3Zn_2]^{2+}$, 429.127); 877.260 ($[C_{43}H_{50}N_8O_3Zn_2F]^+$, 877.253). Anal. (%) Calcd for $C_{45}H_{55}N_8O_6PF_6Zn_2$: C 50.06, H 5.13, N 10.38. Found: C 50.46, H 5.38, N 10.57.

$[Zn_2(L^4)(OAc)_2]PF_6$ (47.5 mg, 50%):. ^1H NMR (CD_3CN, 500.13 MHz): 1.85 (s, 3H, H2a/H4a), 1.94 (s, 3H, H17), 2.05 (s, 3H, H2a/H4a), 3.02 (d, 1H, ^2J = 11.37 Hz, H13/H21), 3.17 (d, 1H, ^2J = 15.77 Hz, H33), 3.24 (d, 1H, ^2J = 15.77 Hz, H33), 3.28 (d, 1H, ^2J = 10.64 Hz, H13/H21), 3.35 (d, 1H, ^2J = 16.51 Hz, H12), 3.50 (d, 1H, ^2J = 16.51 Hz, H12), 3.57 (d, 1H, ^2J = 13.94 Hz, H27), 3.80 (d, 1H, ^2J = 11.37 Hz, H13/H21), 4.03 (d, 1H, ^2J = 14.67 Hz, H6), 4.33 (d, 1H, ^2J = 10.64 Hz, H13/H21), 4.40 (dd, 2H, ^2J = 14.12 Hz, ^2J = 10.09 Hz, H6, H27), 5.58 (d, 1H, ^3J = 7.34 Hz, H31), 5.78 (bs, 2H, NH_2), 6.05 (d, 1H, ^3J = 8.10 Hz, H29), 6.29 (d, 1H, ^4J = 1.83 Hz, H15/H18), 6.45−6.53 (m, 3H, H10, H15/H18, H23), 6.55 (d, 1H, ^3J = 7.34 Hz, H25), 6.67 (bs, 2H, NH_2), 6.88 (dd, 1H, ^3J = 8.44 Hz, ^3J = 7.34 Hz, H30), 6.98−7.03 (m, 1H, H8), 7.33 (td, 1H, ^3J = 7.61 Hz, ^4J = 1.65 Hz, H9), 7.41−7.50 (m, 3H, H2, H4, H24), 7.93 (td, 1H, ^3J = 7.79 Hz, ^4J = 1.65 Hz, H3), 8.28 (m, 1H, H7), 8.72 (m, 1H, H1) ppm. ^{13}C NMR (CD_3CN, 100.62 MHz): 20.19 (C17), 25.03 (C2a/C4a) 25.87 (C2a/C4a), 58.67 (C12), 58.72 (C33), 60.35 (C13/C21), 60.68 (C6), 60.82 (C27), 60.95 (C13/C21), 108.66 (C29), 110.53 (C31), 110.77 (C23/C25), 112.71 (C23/C25), 122.02 (C10), 123.63 (C8), 124.36 (C19/C14), 124.93 (C2/C19/C14), 125.00 (C2/C19/C14), 125.21 (C4/C16), 125.29 (C4/C16), 131.63 (C15/C18), 131.70 (C15/C18), 138.88 (C9), 139.20 (C30), 140.32 (C3), 140.56 (C24), 147.05 (C7), 148.50 (C1), 153.88 (C26/C32), 153.94 (C26/C32), 156.09 (C5/C11), 156.14 (C5/C11), 159.96 (C28), 160.42 (C22), 160.51 (C20), 179.13 (C1a/C3a), 179.31 (C1a/C3a) ppm. ^{31}P NMR (CD_3CN, 100.61 MHz) −144.31 (sep, PF_6^-) ppm. FT-IR spectroscopy (ν, cm^{-1}): 3484 (ν(N−H)), 3332 (ν(N−H)), 3218 (ν(N−H)), 2984 (ν(C−H)), 2935 (ν(C−H)), 2906 (ν(C−H)), 1643 (δ(CNH)), 1606 (ν_a(OAc)), 1476 (ν_s(OAc)), 1275 (ν(C−N)), 827 (ν(P−F)), 658 (δ(py−H)), 557 (δ(F−P−F)). HRMS (ESI^+, CH_3CN): m/z 344.073 ($[C_{33}H_{34}N_8OZn_2]^{2+}$, 344.070); 749.152 ($[C_{33}H_{34}N_8OZn_2CH_3COO]^+$, 749.152). HRMS ($ESI^+$, CH_3OH): m/z 809.177 ($[C_{37}H_{41}N_8O_5Zn_2]^+$, 809.175). Anal. (%) Calcd for $C_{37}H_{41}N_8O_5PF_6Zn_2$: C 46.61, H 4.33, N 11.75. Found: C 46.42, H 4.34, N 11.74.

$[Zn_2(H_2L^6)(OAc)(OH)]$ (85.7 mg, 67%). FT-IR spectroscopy (ν, cm^{-1}): 2978 (ν(C−H)), 2932 (ν(C−H)), 2867 (ν(C−H)), 1681 (ν(C═O)), 1581 (ν_a(OAc)), 1453 (ν(C−$(CH_3)_3$), 1433 (ν_s(OAc)), 1305 (ν(C−N)), 770 (δ(py−H)). HRMS (ESI^+, CH_3CN): m/z 435.6 ($[C_{44}H_{51}N_7O_4Zn_2]^{2+}$, 435.627). Anal. (%) Calcd for $C_{46}H_{55}N_7O_7Zn_2$: C 58.24, H 5.84, N 10.33. Found: C 58.02, H 5.57, N 10.19.

■ ASSOCIATED CONTENT

Ⓢ Supporting Information

The Supporting Information includes details of the crystallographic experiments, ORTEP plots of all molecular structures, the spectroscopic characterization of the compounds used, as well as details on the inhibition studies. CCDC 998887−998891 and CCDC 1009842 contain the supplementary crystallographic data. This material is available free of charge via the Internet at http://pubs.acs.org.

■ AUTHOR INFORMATION

Corresponding Author

*Fax: +49-6221-546617. E-mail: peter.comba@aci.uni-heidelberg.de.

Notes

The authors declare no competing financial interest.

■ ACKNOWLEDGMENTS

Financial support by the German Science Foundation (DFG) and the University of Heidelberg is gratefully acknowledged. We are grateful to Prof. Paul Bernhardt (UQ) for his help with the crystal structure analyses.

REFERENCES

(1) Kimura, E. *Curr. Opin. Chem. Biol.* **2000**, *4*, 207−213.
(2) Weston, J. *Chem. Rev.* **2005**, *105*, 2151−2174.
(3) Mitić, N.; Smith, S. J.; Neves, A.; Guddat, L. W.; Gahan, L. R.; Schenk, G. *Chem. Rev.* **2006**, *106*, 3338−3363.
(4) Jarenmark, M.; Csapo, E.; Singh, J.; Wockel, S.; Farkas, E.; Meyer, F.; Haukka, M.; Nordlander, E. *Dalton Trans.* **2010**, *39*, 8183−8194.
(5) Schenk, G.; Mitić, N.; Hanson, G.; Comba, P. *Coord. Chem. Rev. (Special Issue Ed Solomon)* **2013**, *257*, 473−482.
(6) Carlsson, H.; Nordlander, E.; Jarenmark, M. *C. R. Chim.* **2007**, *10*, 433−462.
(7) Jarenmark, M.; Kappen, S.; Haukka, M.; Nordlander, E. *Dalton Trans.* **2008**, 993−996.
(8) Daumann, L.; Marty, L.; Schenk, G.; Gahan, L. R. *Dalton Trans.* **2013**, *42*, 9574−9584.
(9) Desbouis, D.; Troitsky, I. P.; Belousoff, M. J.; Spiccia, L.; Graham, B. *Coord. Chem. Rev.* **2012**, *256*, 897−937.
(10) Feng, G.; Natale, D.; Prabaharan, R.; Mareque-Rivas, J. C.; Williams, N. H. *Angew. Chem., Int. Ed.* **2006**, *45*, 7056−7059.
(11) de Souza, B.; Kreft, G. L.; Bortolotto, T.; Terenzi, H.; Bertoluzzi, A. J.; Castellano, E. E.; Peralta, R. A.; Domingos, J. B.; Neves, A. *Inorg. Chem.* **2013**, *52*, 3594−3596.
(12) Comba, P.; Gahan, L. R.; Hanson, G. R.; Mereacre, V.; Noble, C. J.; Powell, A. K.; Prisecaru, I.; Schenk, G.; Zajaczkowski-Fischer, M. *Chem.—Eur. J.* **2012**, *18*, 1700−1710.
(13) Comba, P.; Gahan, L. R.; Mereacre, V.; Hanson, G. R.; Powell, A. K.; Schenk, G.; Zajaczkowski-Fischer, M. *Inorg. Chem.* **2012**, *51*, 12195−12209.
(14) Mohamed, M. F.; Brown, R. S. *J. Org. Chem.* **2010**, *75*, 8471−8477.
(15) Suzuki, M.; Kanatomi, H.; Murase, I. *Chem. Lett.* **1981**, *10*, 1745−1748.
(16) Borovik, A. S.; Papaefthymiou, V.; Taylor, L. F.; Anderson, O. P.; Que, L. *J. Am. Chem. Soc.* **1989**, *111*, 6183−6195.
(17) Addison, A. W.; Rao, T. N.; Reedijk, J.; van Rijn, J.; Verschoor, G. *J. Chem. Soc., Dalton Trans.* **1984**, 1349−1356.
(18) Selmeczi, K.; Michel, C.; Milet, A.; Gautier-Luneau, I.; Philouze, C.; Pierre, J.-L.; Schnieders, D.; Rompel, A.; Belle, C. *Chem.—Eur. J.* **2007**, *13*, 9093−9106.
(19) Berreau, L. M.; Saha, A.; Arif, A. M. *Dalton Trans.* **2006**, 183−192.
(20) Matsufuji, K.; Shiraishi, H.; Miyasato, Y.; Shiga, T.; Ohba, M.; Yokoyama, T.; Okawa, H. *Bull. Chem. Soc. Jpn.* **2005**, *78*, 851−858.
(21) Mareque-Rivas, J. C.; Prabaharan, R.; Parsons, S. *Dalton Trans.* **2004**, 1648−1655.
(22) Hough, E.; Hansen, L. K.; Birknes, B.; Jynge, K.; Hansen, S.; Hordvik, A.; Little, C.; Dodson, E.; Derewenda, Z. *Nature* **1989**, *338*, 357−360.
(23) Goldberg, J.; Huang, H. B.; Kwon, Y. G.; Greengard, P.; Nairn, A. C.; Kuriyan, J. *Nature* **1995**, *376*, 745−753.
(24) Hesse, M.; Meier, H.; Zeeh, B. *Spectroscopic Methods in Organic Chemistry*, 2nd ed.; G. Thieme: New York, 1997.
(25) Guenzler, H.; Gremlich, H.-U. *IR Spectroscopy: An Introduction*; Wiley-VCH: Weinheim, 2002.
(26) Nakamoto, K. *Infrared and Raman Spectra of Inorganic and Coordination Compounds, Part B*; Wiley-VCH: New York, 1997.
(27) Daumann, L. J.; Gahan, L. R.; Comba, P.; Schenk, G. *Inorg. Chem.* **2012**, *51*, 7669−7681.
(28) Segel, I. H. *Enzyme Kinetics - Behavior and Analysis of Rapid Equilibrium and Steady-State Enzyme Systems*; Wiley-VCH: New York, 1975.
(29) Kantacha, A.; Buchholz, R.; Smith, S.; Schenk, G.; Gahan, L. *J. Biol. Inorg. Chem.* **2011**, *16*, 25−32.
(30) Mareque-Rivas, J. C.; Prabaharan, R.; de Rosales, R. T. M. *Chem. Commun.* **2004**, 76.
(31) Coburn, S. P.; Mahuren, J. D.; Jain, M.; Zubovic, Y.; Wortsman, J. *J. Clin. Endocrinol. Metab.* **1998**, *83*, 3951−3957.
(32) Fernley, H. N.; Walker, P. G. *Biochem. J.* **1967**, *104*, 1011−1018.
(33) Kinoshita, E.; Takahashi, M.; Takeda, H.; Shiro, M.; Koike, T. *Dalton Trans.* **2004**, 1189.
(34) Daumann, L. J.; Dalle, K. E.; Schenk, G.; McGeary, R. P.; Bernhardt, P. V.; Ollis, D. L.; Gahan, L. R. *Dalton Trans.* **2012**, *41*, 1695−1708.
(35) Gorenstein, D. G. *Phosphorus-31 NMR: Principles and Applications*; Accademic Press: Orlando, FL, 1984.
(36) Sheldrick, G. M.*SHELXS*; University of Göttingen: Göttingen, Germany, 1997.
(37) Sheldrick, G. M. *SHELXL97*; Release 97-2; Universität Göttingen: Göttingen, Germany, 1998.
(38) Carvalho, N. M. F.; Horn, A., Jr.; Bortoluzzi, A. J.; Drago, V.; Antunes, O. A. C. *Inorg. Chim. Acta* **2006**, *359*, 90−98.
(39) Johannsson, A.; Abrahamsson, M.; Magnuson, A.; Huang, P.; Mårtensson, J.; Styring, S.; Hammarström, L.; Sun, L.; Åkermark, B. *Inorg. Chem.* **2003**, *42*, 7502−7511.
(40) Carlsson, H.; Haukka, M.; Bousseksou, A.; Latour, J.-M.; Nordlander, E. *Inorg. Chem.* **2004**, *43*, 8252−8262.
(41) Sun, G.-C.; He, Z.-H.; Li, Z.-J.; Yuan, X.-D.; Yang, Z.-J.; Wang, G.-X.; Wang, L.-F.; Liu, C.-R. *Molecules* **2001**, *6*, 1001−1005.
(42) Lambert, E.; Chabut, B.; Chardon-Noblat, S.; Deronzier, A.; Chottard, G.; Bousseksou, A.; Tuchagues, J.-P.; Laugier, J.; Bardet, M.; Latou, J.-M. *J. Am. Chem. Soc.* **1997**, *119*, 9424−9437.
(43) Jovito, R.; Neves, A.; Bortoluzzi, A. J.; Lanznaster, M.; Drago, V.; Haase, W. *Inorg. Chem. Commun.* **2005**, *8*, 323−327.
(44) Drewry, J. A.; Fletcher, S.; Hassan, H.; Gunning, P. T. *Org. Biomol. Chem.* **2009**, *7*, 5074−5077.
(45) Das, B.; Haukka, M.; Nordlander, E. *Acta Cryst.* **2014**, *E70*, m120−m121.

dx.doi.org/10.1021/ic5009945 | *Inorg. Chem.* 2014, 53, 9036−9051